Heisenberg spin exchange and molecular diffusion in liquid crystals

Akbar Nayeem, S. B. Rananavare, V. S. S. Sastry,[a] and Jack H. Freed
Baker Laboratory of Chemistry, Cornell University, Ithaca, New York 14853-1301

(Received 5 June 1989; accepted 21 August 1989)

Heisenberg spin exchange (HE) studies of translational diffusion of the nitroxide radicals PD-tempone and *P* probe in two liquid crystalline solvents 6OCB–8OCB and 4O,6 are described. It is shown that while PD-tempone undergoes strong exchange in the two solvents, the more anisotropic *P*-probe exhibits a tendency toward weak exchange which becomes more prominent in the low temperature mesophases. The molecular diffusion rates measured from our HE studies are compared with rates measured over larger distances using electron-spin resonance (ESR) imaging methods; we find that, in similar thermotropic liquid crystals, the former are somewhat faster. Also, while diffusion rates for PD-tempone (using HE) in the ordered phases of 6OCB–8OCB are consistent with a single activation energy, those in 4O,6 show variations; suggesting that probe expulsion from core to chain regions in the former most likely occurs prior to S_A formation, whereas in the latter it occurs in the S_A phase. The absence of discontinuities in our diffusion data at the N–S_A–RN transitions supports the belief that these transitions are subtle, with nothing dramatic occurring as the reentrant nematic (RN) phase is formed. The effect of including a potential of mean force $U(r)$ between colliding radicals due to the liquid-crystal structure, is also considered. Our analyses indicate that the potential is of a repulsive nature [i.e., $U(d) > 0$] suggesting the possibility of solvent molecules inhibiting collisions of radicals at distances shorter than the sum of their solvated radii. The influence of orientational ordering on HE involving nonspherical radicals is considered, but changes from strong to weak exchange in the ordered phases appear to depend on how τ_1 the lifetime of the interacting radical pair is influenced by $U(r)$. A careful effort is made to separate the HE effects from the intermolecular electron–electron dipolar (EED) interactions. It is suggested that anomalies in *D* obtained from HE vs EED in this and earlier studies may also be rationalized in terms of the effects of $U(r)$.

I. INTRODUCTION

Heisenberg spin exchange (HE) is a well-established technique used in electron–spin resonance (ESR)[1] for measuring microscopic translational diffusion rates in liquids,[1–4] liquid crystals,[5] and biological membranes.[1,6] Complementary to HE methods, where the extent of line-broadening measures diffusion over dimensions on the order of molecular lengths, are methods that involve diffusion over macroscopic distances. Examples of these latter techniques include fluorescence photobleaching,[7] nuclear magnetic resonance (NMR) field-gradient pulsed methods[8] and ESR imaging.[9] In contrast to macroscopic methods, HE measurements of spin exchange rates (being *microscopic* probes of motion) can provide insight leading to models of molecular dynamics which, when combined with ESR studies of reorientational relaxation, lead to an enhanced understanding of microscopic molecular behavior. Such considerations become especially important when, e.g., there might be several models consistent with a measured rotational diffusion rate and it is necessary to discriminate between them. Furthermore, the translational diffusion (and its anisotropy, which, however, can be directly measured by the new ESR imaging technique,[9] but not by HE experiments) has been shown to play an important role in the spin relaxation near phase transitions in liquid crystals.[10,11]

In this paper, we describe HE studies of translational diffusion rates for two deuterated nitroxide spin probes 2, 2′, 6, 6′ tetramethyl 4-piperidone *N*-oxide (PD-Tempone) and 2, 2′, 6, 6′ tetramethyl 4-butoxybenzoyl amino-piperidone *N*-oxide (*P* probe) in two liquid crystals. The first consists of a binary mixture of 27 wt. % 4-cyano 4′-hexyloxy biphenyl (6OCB) and 73 wt.% 4-cyano 4′-octyloxy biphenyl (8OCB), which for brevity will be referred to as 6OCB–8OCB; the second is *N*-(*p*-butoxybenzylidene) *p*-*n*-hexylaniline (4O,6). 6OCB–8OCB is a liquid crystal exhibiting a bilayer smectic-*A* (S_A) phase followed by a reentrant nematic (RN) phase at lower temperature,[12] whereas 4O,6 exhibits a monolayer S_A phase followed by a S_B phase. The structures of the spin probes and liquid crystals mentioned here (together with the phase transition temperatures of the latter) are shown in Figs. 1 and 2, respectively. The size (and anisotropy) of the spin probes increases in the order PD-tempone < *P* probe. Accordingly, one might expect the diffusion rates to decrease in that order [and in fact, detailed studies of *rotational* dynamics in these systems have shown this to be the case[13]].

The main purpose of this work is to study changes in molecular translational dynamics as the liquid crystals undergo changes in ordering and phase transitions, and thereby reach an improved understanding of the molecular dynamics in these systems. Even though the HE method cannot be used to determine the diffusion constants $D_\parallel$ and $D_\perp$ individually (where $D_\parallel$ and $D_\perp$ denote coefficients for diffusion in

[a] Present address: School of Physics, University of Hyderabad, Hyderabad 500134, India.

 0021-9606/89/236887-19$02.10

Acronym	Name	Structure
PD-Tempone	2,2′,6,6′-tetramethyl-4-piperidine N-oxide (perdeuterated)	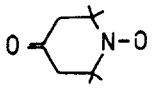
MOTA	4-methylamino-2,2′,6,6′-tetramethyl-piperidinyl-N-oxide (perdeuterated ring)	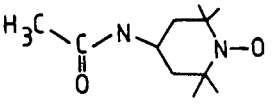
P	2,2′,6,6′-tetramethyl-4-(butyloxy)-benzoylamino-piperidine N-oxide (perdeuterated piperidine ring)	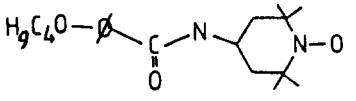
CSL	3′,3′-dimethyloxazolidinyl-N-oxy 2′,3 – 5α-cholestane	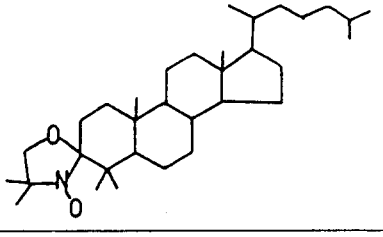

FIG. 1. Structures of some spin probes discussed in this study.

Acronym	Name	Formula
6OCB	4-cyano 4′-n-hexyloxybiphenyl	NC-Φ-Φ-OC_6H_{13}
8OCB	4-cyano 4′-n-octyloxybiphenyl	NC-Φ-Φ-OC_8H_{17}
4O,6	N-(p-butoxybenzylidene)-p-n-hexylaniline	H_9C_4O-Φ-CH=N-Φ-C_6H_{13}
4O,8	N-(p-butoxybenzylidene)-p-n-octylaniline	H_9C_4O-Φ-CH=N-Φ-C_8H_{17}
8CB	4-cyano 4′-n-octylbiphenyl	NC-Φ-Φ-C_8H_{17}
S2	Eutectic mixture of: 50% 4-cyano 4′-n-octylbiphenyl 39% 4-cyano 4′-n-decylbiphenyl 11% 4-cyano 4′-n-decyloxybiphenyl	 NC-Φ-Φ-C_8H_{17} NC-Φ-Φ-$C_{10}H_{21}$ NC-Φ-Φ-$OC_{10}H_{21}$

Transition temperatures of some liquid crystals*

a. 27% 6OCB – 73% 8OCB	K (24°C) N (31°C) S_A (45°C) N (79°C) I
b. 4O,6	K (18°C) S_B (48°C) S_A (55°C) N (78°C) I
c. 8CB	K (21°C) S_A (34°C) N (41°C) I
d. S2	K (-10°C) S_A (48°C) N (49°C) I

FIG. 2. Structures of some liquid crystals referred to in this study with their phase transition temperatures. * Footnotes: (a) Ref. 5; (b) G. W. Smith and Z. G. Gardlund, J. Chem. Phys. **59**, 3214 (1973); (c) G. W. Gray, J. Phys. (Paris) C-**36**, 337 (1975); (d) BDH, Liquid Crystals Catalog.

directions parallel and perpendicular to a laboratory fixed frame, usually chosen to be the mean director in the case of liquid crystals), but rather a mean diffusion constant (D), such measurements nevertheless provide a useful independent check of the molecular models proposed on the basis of reorientational relaxation studies alone. For example, our studies with PD-tempone in several liquid crystals exhibiting S_A phases[13,14] have been consistent with the idea that as smectic layers begin to form, the probe molecules get expelled from the aromatic core regions to the aliphatic chains of the liquid crystals. Translational dynamics of the probes, studied through HE, can be used to investigate whether probe expulsion occurs prior to, or following, the formation of the S_A phase. Furthermore, in the context of reentrant nematic liquid crystals, the study of diffusion rates can be used to discern differences, if any, between the nematic (N) and reentrant nematic (RN) phases.

In all such cases, any changes occurring in the activation energy for translational diffusion as the liquid crystals undergo phase transitions reflect the sensitivity of the probe to changes in the order parameter(s) and/or density that the liquid crystals experience in forming new phases. Since such changes are known to directly affect the spectral densities for relaxation,[10,11] a knowledge of D provides a basis for understanding critical anomalies in spin relaxation.[11] All these considerations emphasize the important role HE studies can play in reaching a deeper understanding of motional dynamics.

Given that liquid crystals are viscous fluids, one finds that the contribution from intermolecular electron-spin dipolar interactions can become a significant concentration-dependent relaxation mechanism.[3–6] It is therefore impor-

tant to be able to distinguish between HE and dipolar contributions. On the other hand, both these mechanisms can, in principle, supply complementary information on the microscopics of diffusion. These are matters that we also address in the present work.

In Sec. II, the theoretical formalism is reviewed. Section III describes the experimental procedures; these include the methods of sample preparation, the ESR spectrometer, and data collection. In Sec. IV we describe the methods of data analysis based on the physical models used. The experimental results are discussed in Sec. V. In the next section (VI), some of our results are analyzed in terms of weak (or intermediate) exchange. Anisotropic effects in spin exchange are also discussed. The main conclusions are summarized in Sec. VII. In Appendix A, we describe a more general theory, the Pedersen–Freed (PF) model, which includes the effects of pair-correlation functions on HE and on dipolar relaxation. An application of the PF theory in simulating the linewidth behavior as a function of solvent viscosity is described. Finally, in Appendix B, we provide a theoretical framework for discussing the effects of orientational ordering on spin exchange involving nonspherical molecules.

II. THEORETICAL BACKGROUND

A. Heisenberg spin exchange

The phenomenon of Heisenberg spin exchange, in which two electron-spin-bearing radicals collide and which effectively results in the electron spins $\mathbf{S}_1$ and $\mathbf{S}_2$ exchanging their nuclear environments, is a time-dependent and diffusion controlled process owing to the relative motion of the radical pairs.[1] During the (bimolecular) collision, the exchange interaction that occurs is described in terms of the Hamiltonian $\mathscr{H}_{ss}$:

$$\mathscr{H}_{ss} = J(t)\mathbf{S}_1\cdot\mathbf{S}_2 \tag{1}$$

where $J(t)$ is twice the (time-dependent) exchange integral. The time dependence of J is taken into account implicitly through the dependence of J on r and Ω_r which specify the distance and orientation of a given radical with respect to another.

A quantity of fundamental interest in HE studies is $\omega_{\rm HE}$, the spin exchange frequency. $\omega_{\rm HE}$ is directly proportional to the concentration of spins in the system. When the solutions are not too concentrated (concentrations below 15 mM in typical fluids), the "slow exchange" condition, characterized by $\omega_{\rm HE} \ll \gamma_e a_{\rm N}$, where $a_{\rm N}$ denotes the isotropic nitrogen hyperfine splitting for nitroxide spin probes and γ_e is the electron gyromagnetic ratio, is usually met.[15] Under these conditions, and assuming a contact exchange model (i.e., that exchange occurs for every bimolecular collision regardless of the relative orientation of the radicals), it has been shown that under strong exchange conditions (see below)[3]

$$\omega_{\rm HE} = \tau_2^{-1} = (\sqrt{3}/2) f_M \gamma_e [\delta_M - \delta_M(0)], \tag{2}$$

where τ_2 is the mean time between successive bimolecular collisions; δ_M and $\delta_M(0)$ are the first derivative ESR intrinsic linewidths of the line of spectral index M in the presence and absence of exchange, respectively. The subtraction effectively eliminates all contributions to spin relaxation that are independent of concentration, leaving only intermolecular mechanisms. In Eq. (2), "M" refers to a given hyperfine line in the spectrum (for ESR spectra from ^{14}N nitroxides $M = 1,0,-1$ correspond to the low, central, and high field lines, respectively), and f_M is a statistical factor related to the degeneracy (and thus intensity) of the spin eigenstates that are involved in the transition describing that line

$$f_M = \frac{N}{(N - 2D_M)}, \quad N = \sum_M D_M. \tag{3}$$

Here, N is the total number of spin eigenstates and D_M denotes the degeneracy of the Mth eigenstate, where M refers to the nuclear spin quantum number identifying the eigenstate(s) involved in the particular ESR transition. For nitroxide radicals (neglecting proton or deuterium superhyperfine splitting), $N = 6$ ($I = 1$, $S = 1/2$) and since the eigenstates are nondegenerate, $D_M = 1$. Therefore, $f_M = 3/2$.

For Brownian diffusion involving neutral radicals, τ_2 is related to the radical diffusion constant D by[3]

$$\tau_2^{-1} = 4\pi d D \mathscr{N}, \tag{4}$$

where d is the encounter distance for two radicals undergoing exchange, D is the self-diffusion coefficient for the radicals, and $\mathscr{N}$ is the number density of radicals[3,4]; ($\mathscr{N}$ is related to the molar concentration C of the solution by $\mathscr{N} = 10^{-3} N_A C$, where N_A is the Avogadro number). Equations (2) and (4) show that, for strong exchange, $d\omega_{\rm HE}/dC$, the slope of the variation of $\omega_{\rm HE}$ with spin concentration, is directly proportional to D. For translational diffusion in isotropic liquids, the Stokes–Einstein relationship gives for self-diffusion[16]

$$D = kT/6\pi r\eta, \tag{5a}$$

where r is the hydrodynamic radius of the diffusing molecule (in HE studies, the spin probe) and η is the absolute viscosity. We shall assume below that $r = d/2$. For diffusion in liquid crystals, it has been suggested that D_s may be visualized as a mean of the diffusion constants $D_\parallel$ and $D_\perp$ [i.e., $D = (D_\parallel + 2D_\perp)/3$] and η may be replaced by an "effective" viscosity, defined as a mean of the viscosities in directions parallel and perpendicular to the magnetic field (5a). It will also be noted that for a Stokes–Einstein hydrodynamic model,

$$D_r = 2kT/3\pi\eta d \tag{5b}$$

for the *relative* diffusion of the radicals.

Equation (2) corresponds to the strong exchange limit, i.e., the situation which obtains when the radical pair is sufficiently long lived that the condition $J_0^2\tau_1^2 \gg 1$ is fulfilled [where τ_1 is the mean lifetime of a radical pair and J_0 is the contact value of $J(r)$]. More generally, however, one has[2]

$$\omega_{\rm HE} = \tau_2^{-1}\left(\frac{J_0^2\tau_1^2}{1 + J_0^2\tau_1^2}\right). \tag{6}$$

In Eq. (6), τ_2 is related to D via Eq. (4), whereas τ_1 is related to D by

$$\tau_1^c = d^2/6D \tag{7a}$$

for a contact exchange model,[17] or

$$\tau_1(\lambda) \approx \frac{d^2}{2D(\lambda d)}\left(1+\frac{1}{\lambda d}\right) \tag{7b}$$

for a model that allows for the finite range of the exchange interaction, i.e., $J(r) = J_0 \exp[-\lambda(r-d)]$.[18] Thus λ specifies the range of the exchange interaction (we shall find it convenient to define $r_{ex} \equiv 5 \ln 10/\lambda$) and d is the distance of closest approach of the radicals. Equations (7a) and (7b) can be generalized to include the effect of interaction potentials between radicals and of the liquid structure via a pair correlation function as discussed later (see Appendix A).

The effect of considering the finite range of exchange is best illustrated with a calculation. Using $d = 12.85$ Å and $J_0 = 8\times10^{10}$ rad/s, parameters that may be considered fairly typical for large nitroxides,[19] ω_{HE} was calculated using Eq. (6) for a solution of spin radical concentration 1.0 mM. Such calculations for a fixed value of $D(0.5\times10^{-6}$ cm^2/s) showed ω_{HE} to have the values 9.60, 9.69, 9.71, and 9.72×10^5 rad/s for $r_{ex} = 1$, 2, 4, and 6 Å, respectively, indicating that, for this example, the effect of the finite range of exchange interaction becomes insignificant at values of r_{ex} exceeding 2 Å.

From Eqs. (4), (6), and (7), we note that as the mechanism of spin exchange changes from strong to weak, the power law dependence of ω_{HE} on D changes from 1 to -1. Therefore, the quantity obtained by measuring the slope of the excess linewidth vs concentration (at a given temperature) will be linearly proportional to D only in the limit of strong exchange, a consideration that will be useful in the context of our experiments with the P probe to be described later.

When the interacting radicals display anisotropic features in their spin exchange, only those collisions for which the colliding radicals are favorably oriented will lead to spin exchange. The measured exchange rate could, therefore, appear smaller than that calculated on the basis of an isotropic exchange model. In this case, the exchange interaction can be described in terms of an orientation-dependent exchange integral $J(r,\Omega_1,\Omega_2)$, where r is the interradical separation, and Ω_1 and Ω_2 are Euler angles specifying the orientation of the two radicals in the laboratory fixed frame.[20] When one of the radicals involved is spherically symmetric, while the other is axially symmetric about some molecular axis, then Zientara and Freed[20] showed that $J = J(r,\theta)$ and they suggested the form

$$J(r,\theta) \cong \left[J_0 + \frac{J_1}{2}(1+\cos\theta)\right] e^{-\lambda(r-d)} \tag{8a}$$

with θ being the angle between the interradical axis and the symmetry axis of the nonspherical radical. In the limit when the anisotropies are averaged out due to rapid rotation of the radicals (see below), Eq. (8a) becomes

$$J(r) = \left(J_0 + \frac{J_1}{2}\right) e^{-\lambda(r-d)}. \tag{8b}$$

The result of Eq. (8a) may be generalized to the case of two interacting nonspherical radicals.[20] In this case, we may write $J = J(r,\theta_1', \theta_2', \phi_1' - \phi_2')$, where θ_i', ϕ_i' denote the polar and azimuthal angles that the p-orbital centered on radical i ($= 1$ or 2) has in a Cartesian coordinate system where the interradical axis is the z axis. A generalization of Eq. (8a) to this case might be

$$\begin{aligned} J(r,\theta_1',\theta_2',\phi_1'-\phi_2') &= J_\sigma \cos\theta_1' \cos\theta_2' [\cos\theta_1' \cos\theta_2' \\ &\quad + \sin\theta_1' \sin\theta_2' \cos(\phi_1'-\phi_2')], \end{aligned} \tag{9a}$$

where J_σ denotes the magnitude of the exchange integral when the two p orbitals on the nitroxide radicals overlap along the interradical axis and is assumed to contain the r dependence [of the same form as in Eq. (8a)]. The polar coordinates of the interradical axis in the lab frame are β and γ, whereas those for the symmetry axes of the ith radical are α_i^0 and β_i^0. Thus, if (θ_i'', ϕ_i'') denote the polar coordinates of the p orbital $N_i - P_i$ in the laboratory frame, we have

$$\cos\theta_i' = \cos\beta\cos\theta_i'' + \sin\beta\sin\theta_i''\cos(\gamma-\phi_i''). \tag{9b}$$

The effect on the magnitude of J of rotation of the spin probes along their symmetry axes is discussed in detail in Appendix B. The important point in these cases is that the molecular orientations are referred to the interradical axis.

When the rotational correlation time of the radical τ_R is shorter than τ_1, the anisotropies may be averaged out during the exchange encounter.[20] Note that in a Stokes–Einstein model,

$$\tau_R = \kappa\tau^*/6 \tag{10}$$

with $\tau^* = \pi\eta d^3/kT$ and where the factor $\kappa \leqslant 1$ allows for a rotational slip of the radicals. In this notation, Eqs. (7) [with Eq. (5b)] become $\tau_1(\lambda) = (3/2)\tau^*(\lambda d)^{-2}(\lambda d + 1)$ and $\tau_1^c = \tau^*/4 = (3/2)\tau_R/\kappa$. Thus, smaller values of κ (i.e., < 1) would lead to the anisotropies of J in Eqs. (8a) and (9a) being averaged out.

In liquid-crystalline phases, the distribution function for the orientation of the ith type of molecule $P(\Omega_i^0)$ is no longer uniform. In general, it is axially symmetric about the preferred direction of alignment, i.e., the nematic director (for a uniaxial liquid crystal). For an axially symmetric molecule, $P(\beta_i^0)$ is no longer uniform. However, even though $P(\beta_i^0)$ may be nonuniform, it is quite possible for $P(\beta)$, the distribution function for the orientation of the interradical axis, to be uniform. (We would expect this to be the case for nematic phases.) In that case, the average of $\cos\beta_i$ over the distribution $P(\beta)$ is seen to be zero, showing that there is no preferential value of the β_i^0 when the radicals collide. However, it also follows from Eq. (9b) that given some initial value of β at the outset of a molecular collision, the nonuniform $P(\beta_i^0)$ will imply incomplete rotational averaging of $\cos\beta_i^0$. Thus, the effective J in a collision will become a function of β and some collisions will have the characteristics of strong exchange, whereas for others it would be weak exchange, provided J is strongly anisotropic (see Appendix B).

The situation in a smectic phase can be complicated further because of the positional order. Thus, the interradical separation vector r, or more precisely its z component (parallel to the nematic director), may be restricted by the

nonuniform smectic distribution function $P(z)$ for the location of the radical with respect to the bilayer normal. Also, diffusion in this lab frame can become very anisotropic,[21] so that collisions for $\mathbf{r}\|z$ are significantly more infrequent than collisions for $\mathbf{r}\perp z$.

B. Dipolar interactions

Besides HE, concentration-dependent line broadening can also arise from dipole–dipole interactions between the electron spins on neighboring radicals. Therefore, a correct measurement of ω_{HE} is possible only when the contribution to the linewidth due to dipolar interactions is known.[1,3] This effect can be estimated using the point-dipole results for the dipolar coupling of spins as discussed elsewhere.[3] The dipolar contributions to linewidth are given by[3,22]

$$T_2^{-1}(\text{dip}) \approx \hbar^2\gamma^4 S(S+1)\frac{5N+8D_M}{24N} J^{(0)}(0) \quad (11a)$$

where $J^{(0)}(0)$, the zero-frequency spectral density, is given by[22,23]

$$J^{(0)}(0) = \frac{48\pi}{15}\cdot\frac{4\mathcal{N}}{27dD} \quad (11b)$$

for a simple diffusive model. The HE contribution to the linewidth, in the strong exchange limit, is [see Eqs. (2) and (3)]

$$T_2^{-1}(\text{HE}) = \left(\frac{N-2D_M}{N}\right)\cdot 4\pi dD\mathcal{N}. \quad (12)$$

The quantities appearing in these equations have been defined previously [Eqs. (3) and (4)]. The relative ratio of dipolar to exchange contributions to the spin relaxation can be calculated from Eqs. (11) and (12) as[3]

$$\frac{T_2^{-1}(\text{dip})}{T_2^{-1}(\text{HE})} = K_M\cdot\left(\frac{1}{dD}\right)^2, \quad (13a)$$

where

$$K_M = \frac{2}{405}\hbar^2\gamma^4 S(S+1)\left(\frac{5N+8D_M}{N-2D_M}\right). \quad (13b)$$

Substitution into Eqs. (13a) and (13b) leads to

$$\frac{T_2^{-1}(\text{dip})}{T_2^{-1}(\text{HE})} = 0.3762\times 10^{-26}\left(\frac{1}{dD}\right)^2. \quad (13c)$$

Owing to the greater viscosity of solutions at lower temperatures, the role of $T_2^{-1}(\text{dip})$ becomes more important at lower temperatures. For nonspherical molecules and for those spin-bearing molecules where the spins are off center, there are orientational corrections to the dipolar interactions which have been discussed elsewhere.[24] Furthermore, there are likely to be important effects due to the interaction between radicals and the liquid crystal structure via the pair correlation function (see Appendix A).

III. EXPERIMENTAL

A. Materials

The two spin probes PD-tempone and *P* used in this study are shown in Fig. 1. PD-Tempone was prepared using the techniques described by Hwang *et al.*,[25] while the *P* probe was prepared by Dr. Sidney Wolfe. The liquid crystals 6OCB and 8OCB (Fig. 2) were purchased from BDH Chemicals Ltd. and used without further purification. The sample consisting of 27.2% 6OCB in 8OCB (by weight) was prepared by weighing sufficient quantities of the components that concentrations were known to within 0.1% by weight. 4O,6 was prepared in these laboratories by Dr. E. Igner by condensing equimolar quantities of 4-*n* butoxy benzaldehyde and 4-*n* hexyl aniline, followed by recrystallization from absolute ethanol till a constant melting point was achieved.[26]

All the radical solutions were prepared gravimetrically as follows: First, a stock solution of the most concentrated solution used in the study was prepared. To this was added successive amounts of the liquid crystal solvent, thus diluting the solution to the required concentrations as needed. All samples thus prepared were degased using the freeze–pump–thaw cycle to remove oxygen and were then sealed off under a pressure below 0.1 mTorr. The absolute concentrations of the solutions were determined with reference to the most dilute of the solutions, in which no spin exchange was assumed to have occurred. The latter solution was calibrated for spin concentration against a standard solution of PD-tempone in toluene using the standard procedure of comparing integrated intensities.

B. ESR spectrometer

All measurements were performed on a Varian E-12 continuous wave *X*-band spectrometer using 25 kHz field modulation, or 100 kHz when needed. The microwave field modulation amplitude was set at a value less than 10% of the linewidth in order to prevent line shape distortion. Variable temperature experiments were performed using a Varian E-257 variable temperature control unit, with which a long term stability of $\pm 0.5°$ could be attained using dry nitrogen gas as the medium of heat transfer. The copper–constantan thermocouple junction, which was used for temperature measurements, was placed just above the active microwave region.

C. Linewidth measurements

All linewidth measurements were made on a Varian E-12 spectrometer interfaced to a Prime 850 time-shared computer. The spectra were collected with the microwave power set well below the saturation limit. The intrinsic linewidths for each of the three hyperfine lines of the exchange-free samples [i.e., $\delta(0)$ in Eq. (2)] were obtained by fitting each line to a superposition of Lorentzian lines separated by a_D, the deuterium coupling constant (14). Thus, each ^{14}N hyperfine line was simulated by calculating the envelope of superhyperfine lines due to the dipolar coupling of the electron spin to the neighboring 12 methyl deuterons, all assumed to possess the same coupling constant a_D. The coupling of the electron spin to the ring deuterons is known to be much smaller.[25,27] Although such an assumption seems reasonable for PD-tempone, the neglect of electron-spin coupling to the ring deuterons and treating the axial and equatorial deuterons as equal has been seriously questioned in the case of a

larger spin probe somewhat similar to P (but smaller).[5(b)] We have noted that coupling to the ring deuterons does not significantly affect the measured intrinsic linewidth,[28] and the effects of any such couplings are reduced even further when the observed linewidths are larger than 1 G (which was the case with the P probe as noted below). We therefore used the same procedure for obtaining the intrinsic widths for both radicals. The intrinsic linewidths in the presence of spin exchange, δ in Eq. (2), were obtained by a procedure described in the following section.

IV. ANALYSIS

A. HE frequencies and ESR line shapes

With the onset of spin exchange, the widths of the superhyperfine lines within a given ^{14}N hyperfine manifold (i.e., the intrinsic widths) increase, till a point is reached when ω_{HE} becomes large enough that the slow exchange condition with respect to the deuterium coupling frequency, i.e., $\omega_{HE} \ll |\gamma_e| a_D$, is no longer fulfilled. (For PD-tempone, for which $a_D \sim 20$ mG, $|\gamma_e| a_D \approx 3.5 \times 10^5$ rad/s) Under these conditions, the deuterium superhyperfine lines collapse into a single line and the method used for obtaining the intrinsic widths for the exchange-free line described in the previous section is unsuitable. Though the observed linewidth is then very nearly equal to the intrinsic width, the intrinsic widths for the lines in the presence of spin exchange require other methods discussed in detail elsewhere,[2] which we briefly summarize here. For a given nitrogen hyperfine line of spectral index N (1,0 or -1), the spectrum is given by

$$\mathcal{J}_N(\omega) = \mathrm{Im} \sum_M Z_{N,M}(\omega), \tag{14}$$

where $Z_{N,M}(\omega)$ is the power absorbed (at frequency ω) by the transition specified by N and M, the nuclear spin quantum numbers for nitrogen and deuterium coupling, respectively. $Z_{NM}(\omega)$ is determined by solving the matrix equation

$$\left[\Delta\omega_{N,M} - i[T_2(0)^{-1} + \omega_{HE}(1 - P_M/3)]\right] Z_{N,M} + i\omega_{HE} \times P_M \sum_{M'} Z_{N,M'} = D_M A_{N,M}. \tag{15}$$

In Eq. (15), $P_M = D_M/\Sigma_{M'} D'_M$ is the normalized statistical weight of the Mth hyperfine line and D_M is its degeneracy.[3] Also, $\Delta\omega_{N,M} = \omega - \omega_{N,M}$, with $\omega_{N,M}$ being the Larmor frequency of the N,Mth line. The constant $A_{N,M}$, which in the absence of saturation is linear in the microwave field strength, is given by $A_{N,M} = q\omega_{N,M} d_{N,M}$, where $q = h/2\pi kTN$, $d_{N,M} = \gamma B_1/2$, and N represents the total number of spin eigenstates.[29]

Equation (15) is symmetrized using the transformation

$$\tilde{Z}_{N,M} = Z_{N,M} P_M^{-1/2} \tag{16}$$

and premultiplying the resulting equation $P_M^{1/2}$.[30] The symmetric equation then becomes

$$[T_2(0)^{-1} + 2/3\omega_{HE} - i\Delta\omega_{N,M} P_{M'}] \tilde{Z}_{N,M} - \omega_{HE} \sum_{M'} \sqrt{P_M P_{M'}}\, \tilde{Z}_{N,M'} = P_M^{1/2} A_{N,M}. \tag{17a}$$

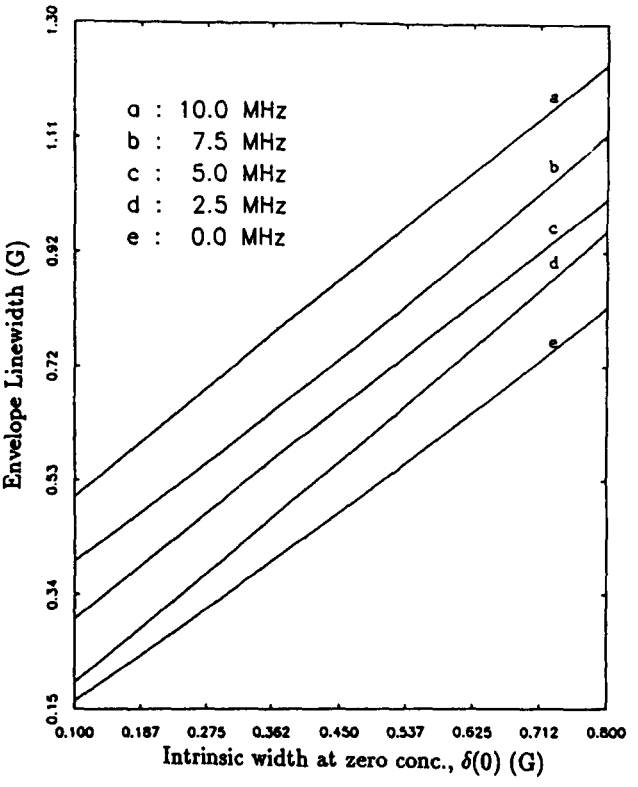

FIG. 3. Calculated envelope linewidth for different values of $\delta(0)$ at the values of ω_{HE} as indicated.

In Eq. (17a), $T_2(0)^{-1}$ is the relaxation rate that corresponds to the exchange-free intrinsic linewidth, and from Eq. (2) it follows that

$$T_2^{*-1} \equiv \frac{\sqrt{3}}{2}|\gamma_e|\delta = (T_2(0)^{-1} + \frac{2}{3}\omega_{HE}) \tag{17b}$$

corresponds to the intrinsic linewidth in the presence of exchange. In Eq. 17(b), δ is the derivative intrinsic linewidth in Gauss. The spectrum is then calculated using the expression

$$\mathcal{J}(\omega) \propto \mathrm{Im} \sum_M \left[\frac{(O^\dagger U)_M^2}{\Lambda_M - i(\omega - \omega_e) + T_2(0)^{-1}}\right]. \tag{18}$$

Here O refers to the complex orthogonal matrix which diagonalizes the matrix equation [Eq. (17)] whose eigenvalues are Λ_M. The physical significance of the eigenmodes is that the $\mathrm{Re}(\Lambda_M)$ and $\mathrm{Im}(\Lambda_M)$ correspond to the linewidth and line position, respectively, of the Mth hyperfine line within a nitrogen manifold and $(O^\dagger U)_M^2$ determines the contribution of that line to the spectral intensity. U is the column vector of P_M's appearing on the right-hand side of Eq. (17a). Figure 3 shows a plot of the envelope linewidth, obtained from the line shape calculated using Eq. (18), as a function of $(\sqrt{3}\gamma_e/2)^{-1} T_2(0)^{-1}$ at several values of ω_{HE}. The utility of Fig. 3 lies in that, for a given observed width in presence of exchange, it is possible to read off directly the value of ω_{HE} if $\delta(0)$ is known at the same temperature.

In order to obtain ω_{HE} at a given temperature, it is necessary to compare the linewidths in the presence and absence of exchange at the *same* temperature. This was accomplished as follows: First, the linewidth vs temperature

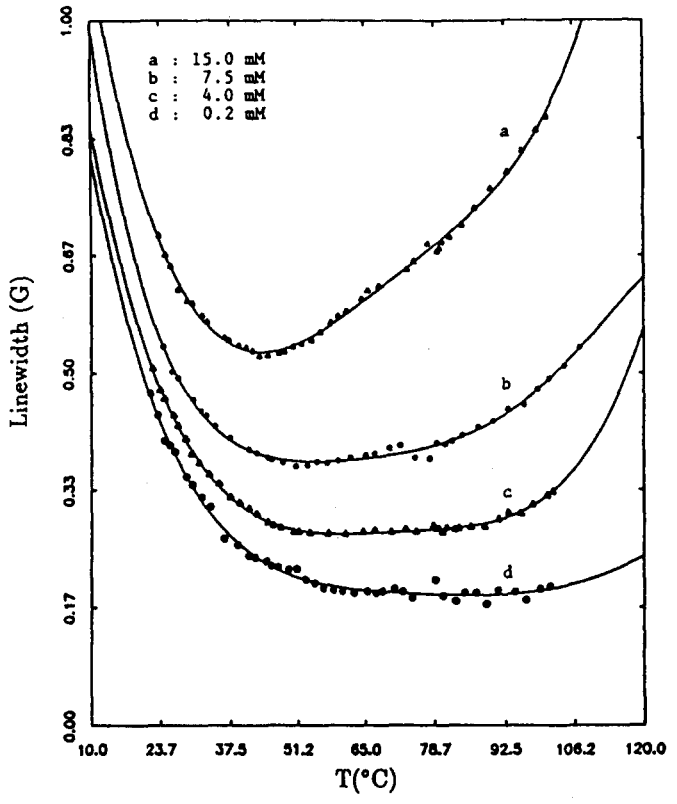

FIG. 4. PD-tempone in 6OCB–8OCB. ESR linewidth [$\delta(C)$] variation with temperature and concentration.

data for each of the concentrations was fitted to a spline. The experimental linewidths at a given temperature were then obtained by reading off the value of the ordinate (linewidth) corresponding to that temperature. An example of such curve fitting is shown in Fig. 4. [In some cases, however (P probe in 4O,6 and 6OCB–8OCB), such comparisons necessitated using (T–T_{NI}) or (T–T_{NA}) rather than T, since the mesomorphic phase transition temperatures were significantly different for the samples of different concentration]. The points in Fig. 4 denote experimental peak-to-peak linewidths at the indicated temperatures and the line through them is the fitted function. Figure 4 makes possible a comparison of solutions of differing concentration at the same temperature.

The intrinsic linewidth of the exchange-free line is obtained as described in Sec. IIIC. The same computer program also gives a_D. Using the intrinsic widths $\delta(0)$ and a_D's thus obtained, we calculated the line shape from Eq. (17a), from which the linewidth of the envelope was obtained. This was repeated for a range of values of ω_{HE}, as illustrated in Fig. 3. Thus, at a given temperature, the exchange frequency may be read off directly (or interpolated) from a knowledge of the observed linewidth and $\delta(0)$.

B. Diffusion constants and activation energies

From Eqs. (11) and (12), we note that the excess linewidth, which is determined by the sum of HE and dipolar contributions, is given by the sum of two terms that, respectively, depend directly and inversely on the diffusion coefficient D. Assuming the temperature dependence of D to be Arrhenius-like, the expected temperature dependence of the excess linewidth may be analyzed in terms of the relation

$$W \equiv \delta - \delta(0) = [A \exp(-\Delta E_{act}/kT) + B \exp(\Delta E_{act}/kT)]C, \tag{19a}$$

where, in Eq. (19), W denotes the excess peak-to-peak derivative linewidth and ΔE_{act} is the activation energy for translational diffusion. A and B are two constants that are independent of concentration C and, for simplicity, are also taken to be independent of temperature (however, more generally, they may depend on temperature as discussed later). The concentration dependence is eliminated by considering the derivative dW/dC, which has the dimensions of a rate constant k:

$$k \equiv \frac{dW}{dC} = A \exp(-\Delta E_{act}/kT) + B \exp(\Delta E_{act}/kT). \tag{19b}$$

The ratio of the two terms on the right-hand side of Eq. (19b) [or Eq. (19a)] represents the relative contributions of HE and dipolar interactions to the linewidth as shown in Eq. (18a) above. Using Eqs. (11) and (12), we calculate, for nitroxide radicals

$$A = 3.31 \times 10^{14}(dD_0) \tag{20a}$$

and

$$B = 1.24 \times 10^{-12}\left(\frac{1}{dD_0}\right). \tag{20b}$$

In these expressions, D_0 is the preexponential factor in the Arrhenius expression for the diffusion coefficient [$D = D_0 \exp(-\Delta E_{act}/kT)$].

The determination of dD_0 and ΔE_{act} for each system was performed in two stages: First, at a given temperature, the slope of the excess derivative linewidth with respect to spin radical concentration (dW/dC) was obtained through a linear regression analysis of the linewidth vs concentration data. The values of dW/dC at different temperatures were then fit to Eq. (19b) using a nonlinear least-squares routine[31] in which the parameters A, B, and ΔE_{act} were adjusted to the lowest χ^2.[32] Using the Eqs. (20a) and (20b), dD_0 could then be obtained either from A, which corresponds to the HE contribution, or from B, the dipolar contribution. In general, we noted that the values of dD_0 calculated from B were two to four times higher than those calculated using A.[32] A possible reason for this discrepancy may be that, more rigorously, the dipolar term should include a factor $e^{-U(d)/kT}$ which reflects the effective interradical potential of mean force $U(r)$ [cf. Appendix A; the larger value of B for our data, in the strong exchange limit, corresponds to $U(d) \sim 1.0$ kcal/mol]; this has been ignored in the above analysis. We therefore used Eq. (20a) to calculate dD_0 (and hence D). The results of all such analyses are shown in Table I, while in Table II we indicate, at given temperatures for different mesophases, the relative contribution of HE to dipolar effects and the diffusion coefficient at that temperature assuming a probe radius of 3.2 Å for PD-tempone and 5.23 Å for P.

TABLE I. Nonlinear least-squares analysis of fits to $k = Ae^{-\Delta E_{act}/RT} + BE^{\Delta E_{act}/RT}$.

System	Phase	$A(G/M)$	$B(G/M)$	ΔE_{act} (kcal/mol)
PDT/4O,6	I	$(1.9 \pm 0.1) \times 10^6$	$(9.7 \pm 0.6) \times 10^{-5}$	(8.06 ± 0.06)
	N	$(5.3 \pm 0.5) \times 10^3$	$(3.5 \pm 0.3) \times 10^{-2}$	(3.70 ± 0.06)
	S_B	$(6.8 \pm 1.2) \times 10^5$	$(1.6 \pm 0.3) \times 10^{-4}$	(6.56 ± 0.12)
PDT/6OCB–8OCB	I	$(1.9 \pm 0.1) \times 10^4$	$(1.7 \pm 0.1) \times 10^{-2}$	(4.42 ± 0.04)
	N,S_A,RN	$(9.5 \pm 3.0) \times 10^3$	$(1.4 \pm 0.4) \times 10^{-2}$	(3.82 ± 0.22)
P/4O,6	I	$(5.4 \pm 0.5) \times 10^6$	$(4.4 \pm 0.4) \times 10^{-5}$	(9.16 ± 0.08)
	N	$(1.3 \pm 0.3) \times 10^8$	$(1.5 \pm 0.4) \times 10^{-6}$	(10.88 ± 0.16)

V. RESULTS

A. PD-tempone in 6OCB–8OCB

The results of our nonlinear least-squares analysis of k vs T are shown in Fig. 5 and for which the fitting parameters A, B, and ΔE_{act} are tabulated in Table I. Corresponding to different temperatures representative of the I, N, S_A, and RN phases, the relative contributions of HE vs dipolar effects and the diffusion constants are shown in Table II. The data in the isotropic phase are consistent with a translational diffusion activation energy of 4.4 kcal/mol, whereas the data in the N, S_A, and RN phases, which appear to be fairly smooth without any abrupt discontinuities, show an activation energy of about 3.8 kcal/mol in these phases.[33] The observed continuous change in the diffusion constant is consistent with our earlier assertion that any molecular changes that occur in the sequence N–S_A–RN are very subtle, with nothing dramatic occurring at these transitions.[13]

The diffusion constants for PD-tempone in 6OCB–8OCB are somewhat larger than those for liquid crystal self-diffusion, which were obtained using other techniques in similar thermotropics. This is presumably due to the smaller size of PD-tempone. As an example, Leadbetter *et al.*,[34] using quasielastic neutron scattering, have measured the self-diffusion rate in 5CB (*p*-pentyl-*p'*-cyanobiphenyl), and find $D_\perp = 4.1 \times 10^{-7}$ cm^2/s and $D_\parallel = 5.3 \times 10^{-7}$ cm^2/s at 25 °C, whereas we find that for PD-tempone in 6OCB–8OCB, $D \approx 7.9 \times 10^{-7}$ cm^2/s at approximately the same temperature (see Table II). From Eq. (5b), we estimate that $D_{tr}(\text{PDT})/D_{tr}(5\text{CB}) = r(5\text{CB})/r(\text{PDT}) \approx 2.0$, so that Leadbetter's results suggest that $D_{tr}(\text{PDT}) \approx 0.9 \times 10^{-6}$ cm^2/s in 5CB. This is very close to the diffusion rate we measure in the reentrant nematic phase of 6OCB–8OCB at 28 °C using HE.

Our results, which correct for the dipolar contributions to line broadening, show that whereas in the isotropic phase the HE term contributes about 83% to the excess linewidth at 85 °C, the contribution of HE to line broadening is somewhat enhanced in the nematic phase, and then decreases as the temperature is lowered. Thus, in the nematic phase HE contributes nearly 88% at 60 °C, which then decreases to 77% in the S_A phase at 40 °C, followed by 68% in the RN phase at 28 °C. Though the relative decrease in the contribution of the HE term to line broadening as temperature is lowered in the mesophases can be understood on the basis of the fact that HE decreases with temperature, while dipolar relaxation increases, the dramatic increase in the HE/dipolar contributions at the *I–N* transition probably indicates that (at least in this case) the exchange mechanism is anisotropic.[20] The enhanced ordering of the radicals causes the PD-tempone molecules to align in an orientation that is particularly favorable to spin exchange.

Finally, it must be pointed out that the actual value of the diffusion constant obtained by this procedure depends on

TABLE II. Dipolar contributions and diffusion coefficients.

System	Phase	T(°C)	$T_2^{-1}(\text{HE})/T_2^{-1}(\text{dip})$	$D \times 10^6$ (cm^2/s)[a]
PDT/4O,6	I	85	3.30	1.16
	N	70	3.14	1.14
	S_B	40	3.39	0.91
PDT/6OCB–8OCB	I	85	4.88	1.87
	N	60	7.10	1.45
	S_A	40	3.42	1.01
	RN	28	2.10	0.79
P/4O,6	I	85	0.95	0.44
	N	70	1.47	0.49
	S_B	40	···	<1.23[b]
P/6OCB–8OCB	I	85	···	<0.77[b]
	N	60	···	<0.78[b]

[a] Calculated from the HE contribution ($A \exp^{-E/RT}$) and assuming $d = 6.4$ Å and $d = 10.46$ Å for PD-tempone and *P*, respectively.

[b] Determined from weak exchange and neglecting dipolar contributions.

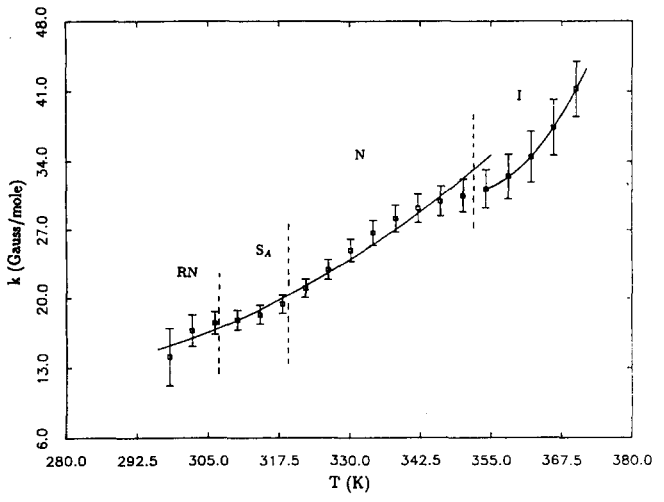

FIG. 5. PD-tempone in 6OCB–8OCB: k vs temperature.

the assumed encounter distance for exchange. We used a value of 6.4 Å, which is twice the value of the crystallographic radius of PD-tempone[25] (3.2 Å). This can, in fact, lead to a significant error in the actual value of D. For example, studies on the translational diffusion of di-tertiary butyl nitroxide (DTBN) in water using a capillary diffusion method[35] indicated that $D = 7.2\times10^{-6}$ cm^2 s^{-1} at room temperature. Berner and Kivelson,[4] who studied the HE, found that $dD = 3.2\times10^{-12}$ cm^3 s^{-1}. Equating the two results gives an encounter distance d of 4.6 Å, whereas the value of d determined from space filling models is 6.3 Å. [A model that might explain this discrepancy is discussed in Appendix A.]

B. PD-tempone in 4O,6

4O,6 has two smectic phases: S_A, which consists of layers of aligned molecules in planes normal to the main ordering axis (the director) and the S_B phase, which in addition to the symmetry of S_A possesses hexagonal symmetry within each smectic layer.

The analysis leading to the diffusion constants and activation energies is summarized in Tables I and II, and our fits to the experimental data are shown in Fig. 6. It is noted that:

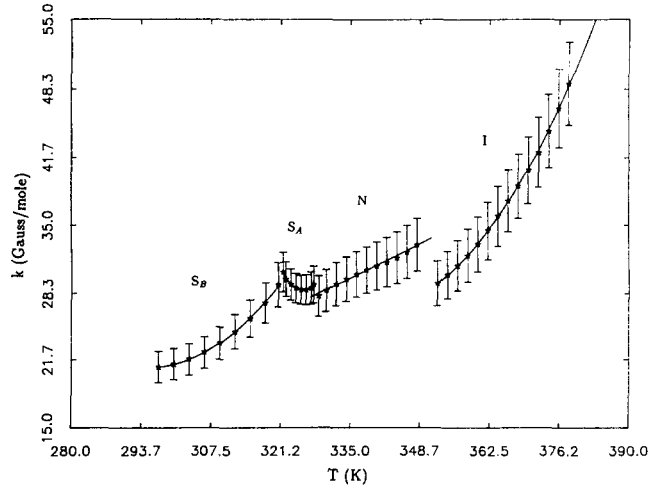

FIG. 6. PD-tempone in 4O,6: k vs temperature.

(i) Translational diffusion rates in the isotropic and nematic phases appear to be comparable. Owing to the relatively narrow width of the S_A phase (6–7 °C), a satisfactory analysis in terms of A and B could not be performed. On lowering the temperature into the S_B phase, the diffusion rate (at 40 °C) decreases to about 0.9×10^{-6} cm^2/s.

(ii) Unlike in 6OCB–8OCB, where the translational diffusion activation energies are comparable in the isotropic and ordered phases, the activation energies appear to change quite notably on passing from one phase to another, dropping sharply from the isotropic value of 8.1 to 3.7 kcal/mol in the N phase, then increasing to 6.6 kcal/mol in the S_B phase.

The results of $D\sim1\times10^{-6}$ cm^2/s obtained for PD-tempone in 4O,6 (cf. Table II) may be compared with the results obtained by ESR imaging for tempone diffusion in related liquid crystals 5,4 (*p*-pentyl benzylidene *p*-butylaniline) and MBBA [N-(p-methoxy benzylidene) *p*-butylaniline], also called 1O,4. For the former, Hornak *et al.*[9(a)] measured $D = 2.5\times10^{-6}$ cm^2/s in the isotropic phase at 50 °C, and $D_\perp = 0.90\times10^{-6}$ cm^2/s, $D_\parallel = 0.64\times10^{-6}$ cm^2/s in the nematic phase at 27 °C. For the latter, Moscicki *et al.*[9(c)] measured $D_\perp = 2.5\times10^{-7}$ cm^2/s and $D_\parallel = 3.7\times10^{-7}$ cm^2/s in the nematic phase at 20 °C. Also, for the mixed liquid crystal phase V, Cleary *et al.*[9(b)] obtained $D_\perp = 1.27\times10^{-7}$ cm^2/s at 22 °C in the nematic phase. When our results of D from HE measurements (Table II) are extrapolated to these temperatures using the activation energies shown in Table I, we find that in the "isotropic phase" at 50 °C, $D\sim0.58\times10^{-6}$ cm^2/s, and in the "nematic phase" at 25 °C, $D\sim0.57\times10^{-6}$ cm^2/s. The result in the nematic phase is somewhat higher (implying faster diffusion) than that measured by imaging. Any further comparison would require results from imaging experiments using 4O,6 as a solvent.

Moseley and Loewenstein,[8] who have studied the diffusion of methane in 7CB and 8CB, and in 4O,6, have shown that smectic-forming nematics have $D_\perp > D_\parallel$. This observation in spite of the apparent isotropy of methane, was attributed to the possible formation of cybotactic smectic clusters (within the nematic phase). This causes the (relatively bulky) aromatic cores to get aligned in layers, thus inhibiting the diffusion of methane across the layers ($D_\parallel$), while not significantly affecting diffusion rates between them ($D_\perp$). Such may well be the case with PD-tempone too. Clearly this effect will be most pronounced near the N–S_A transition, where density fluctuations may appreciably modulate diffusion in directions normal to the smectic planes.[11]

Chu and co-workers[21] have calculated and measured a value of N, the ratio of $D_\parallel$ to $D_\perp$, close to zero in the S_A phase (for spherical particles)! This large anisotropy is probably due to the fact that jumps perpendicular to the smectic layers ($D_\parallel$) are highly restricted owing to a large potential barrier. Such jumps are presumably similar for the impurity and the liquid crystals molecules themselves. Diffusion parallel to the layers, leading to $D_\perp$, occurs between layers in the region of the alkyl chains where there is less hindrance to movement.

In the S_B phase, the diffusion coefficients for methane in 4O,6 are lower than in S_A (i.e., slower motion) and ΔE_{act} for

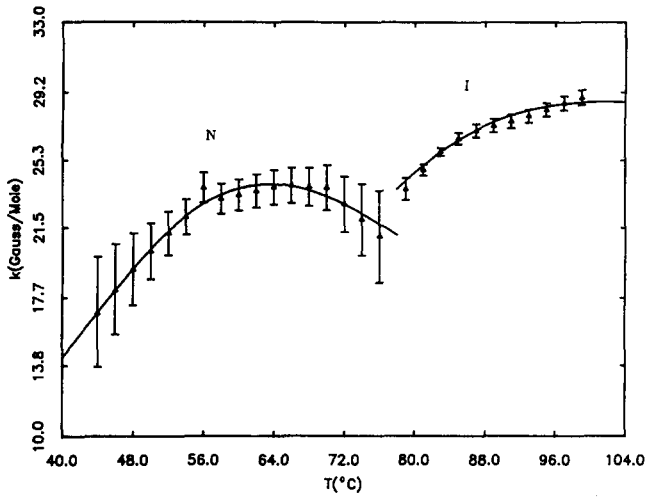

FIG. 7. The P probe in 6OCB–8OCB (I and N phases): k vs temperature.

$D_{\|}$ in S_B is lower than in S_A. Presumably there is less hindrance to diffusion perpendicular to the planes here. The diffusive behavior in the S_B phase has been explained by Kruger[36] qualitatively based on the hypothesis that in S_B, diffusion is a solidlike process which extends in all directions, though still remaining faster along layers ($D_{\perp}$) than perpendicular to them ($D_{\|}$).

The increase in k noted in the S_A phase as the S_B phase is approached is consistent with the result of Moseley and Loewenstein that in the S_A phase of 4O,6, $D_{\perp}$ for methane was found to increase on lowering the temperature. It appears that the influence of increasing smectic ordering tends to decrease the activation energy for transverse diffusion, and in addition, the increased layer packing expels the PD-tempone molecules towards the alkyl chains (from the aromatic regions). Such an argument has proven successful in explaining anomalous ordering and relaxation data.[14] It may also be argued that the exchange mechanism that measures diffusion rates in the S_A phase is highly anisotropic, and that upon entering the S_B phase, where probe expulsion into the alkyl regions is essentially complete, the probes experience a more "isotropic" environment. Furthermore, since the diffusion is then mainly confined to the two-dimensional plane between smectic layers, spin exchange may occur more efficiently. {This latter statement follows in part from the fact that for two-dimensional spin exchange, Zientara and Freed[37] have shown that the radical-pair lifetime (τ_1) gets scaled by the factor ($\ln y_N$), where y_N is related to the position of the boundary walls. For an infinite two-dimensional sheet, the proper results are obtained by taking the limit $y_N \to \infty$, thus causing the effective τ_1 to approach infinity. This increase in effective τ_1, when the dimensionality changes from 3 to 2 can enhance the exchange rate [Eq. (6)].}

C. *P* probe in 6OCB–8OCB

The ESR spectra for the longer and more anisotropic radical, *P* probe (Fig. 1) in 6OCB–8OCB show three well separated hyperfine lines in the nematic and isotropic phases. In the S_A phase, the lines get somewhat broader and show a tendency to merge together at the wings—a typical signature of incipient slow motion. In the reentrant nematic phase, which occurs at temperatures below 31 °C, the spectra are slow motional.

Our data for k vs T are shown in Fig. 7 for the isotropic and nematic phases. In both the isotropic and nematic phases, our fits to the data required the use of a weak exchange model, for possible reasons that we discuss here. The results are shown in Tables II and III.

Although attempts at fitting the isotropic data at the higher temperatures were partially successful using a strong exchange model, we were unable to reproduce the sharply increasing slope (yielding lower k values) as the I–N transition was approached. On the other hand, using a weak exchange model (see Sec. VI A), we were able to fit the data over the entire temperature range in the isotropic phase (cf. Fig. 7).

The data for k in the nematic phase exhibit an *increasing* rather than a decreasing slope as the temperature of the system is lowered, thus completely precluding an analysis using Eq. (19b) as was used for the other systems. The unusual shape can only be rationalized on the assumption that as the temperature of the system is lowered, either (i) the exchange mechanism changes from weak to strong, or (ii) the contribution of strong HE (compared to dipolar effects) increases. However, with decreasing temperature, since HE is known to decrease and dipolar relaxation to increase, the latter pos-

TABLE III. (A) Nonlinear least-squares analysis of fits to $k'' = A''e^{E/RT} + B''e^{-E'/RT}$. (B) $(J_0\tau_1)^2$ and diffusion coefficients.

(A) System	Phase	$A''(M/G)$	E(kcal/mol)	$B''(M/G)$	E'(kcal/mol)
P/4O,6	S_B	$(1.1 \pm 0.1)\times 10^{-10}$	(11.4 ± 0.1)	$(3.4 \pm 0.4)\times 10^{3}$	(7.7 ± 0.1)
P/6OCB–8OCB	I	$(5.9 \pm 1.3)\times 10^{-10}$	(12.2 ± 0.2)	(4.3 ± 0.6)	(3.78 ± 0.08)
	N	$(0.94 \pm 0.01)\times 10^{-10}$	(12.6 ± 0.05)	$(2.27 \pm 0.02)\times 10^{2}$	$(6.01) \pm 0.01)$

(B) System	Phase	T(°C)	$(J_0\tau_1)^2$	$D\times 10^6$(cm^2/s)[a]
P/4O,6	S_B	40	0.68	1.23
P/6OCB–8OCB	I	85	0.77	0.77
	N	60	0.63	0.78

[a] Upper limits only.

sibility can be ignored. The consideration of weak exchange implies that Eq. (12) (which assumes strong exchange) cannot be used in the present case, but must be replaced by the more general expression [Eq. (6)], which considers the finite lifetime of the colliding pair and the overlap integral. Although these matters are discussed in detail in the following section (Sec. VI), we may point out here that we were able to fit the data successfully with Eq. (6). The fits support the hypothesis that as the temperature of the system is lowered, the mechanism changes from weak to strong exchange. In these fits, dipolar contributions to the excess linewidth were neglected, since the inclusion of dipolar terms [i.e, $Be^{E/RT}$ in Eq. (19b)] in these cases involving weak exchange did not lead to convergent results. The diffusion rates measured from such an analysis were found to be somewhat lower than those for PD-tempone in 6OCB–8OCB (Table II), but the values shown are regarded as only upper limits (since any possible dipolar contributions were ignored).

The spectra in the S_A and RN phases at the lowest and highest concentrations were virtually identical; i.e., within the experimental resolution, no line broadening with concentration should be discerned. The observed insensitivity of the linewidth to concentration in the S_A and RN phases (which as noted below was also partially observed with *P* in the S_A phase of 4O,6,) suggests that the diffusion rates significantly drop in the S_A phase. A possible reason for this may be that within the S_A and RN phases, the probe molecules are surrounded by clusters of solvent molecules, so that in these phases diffusion now involves the movement of a larger entity. For efficient spin exchange, the radicals must approach each other sufficiently close for orbital overlap to occur and this could be inhibited by the solvation shells surrounding each radical.

D. *P* probe in 4O,6

Spin relaxation studies performed by Meirovitch *et al.*[38] have shown that the rotational correlation times for *P* in 4O,6 are shorter than in 6OCB–8OCB, falling in the motionally narrowed dynamic regime. Correspondingly, unlike *P* in 6OCB–8OCB, the ESR spectra show three well-resolved hyperfine lines throughout the entire temperature region of interest.

Our results are summarized in Tables I and II, while our best fits to the experimental data in the I and N phases, assuming strong exchange and dipolar relaxation, are shown in Fig. 8. The activation energies for translational diffusion are 9.2 and 10.9 kcal/mol in the isotropic and nematic phases, respectively. The observation that the activation energies for translational diffusion are not very different in the two phases is consistent with the findings of Noack for the NMR self-diffusion of MBBA.[39] On cooling from 85 to 70 °C (I→N phase), the relative HE contribution increases (from 49% to 60%). In both phases, the data seem to be consistent with strong exchange. Using Eq. (19b), however, we were unable to fit the data in the S_A and S_B phases. The linewidth behavior in the S_B phase is qualitatively similar to that observed in the N phase of 6OCB–8OCB with the *P* probe, and for which weak exchange was indicated. Using a weak exchange model to fit our data (described below), but which neglects the effects of dipolar relaxation, we were able to obtain a satisfactory fit to the data. An upper limit for the diffusion coefficient at 40 °C (S_B phase) of about 1.2×10^{-6} cm^2/s was obtained.

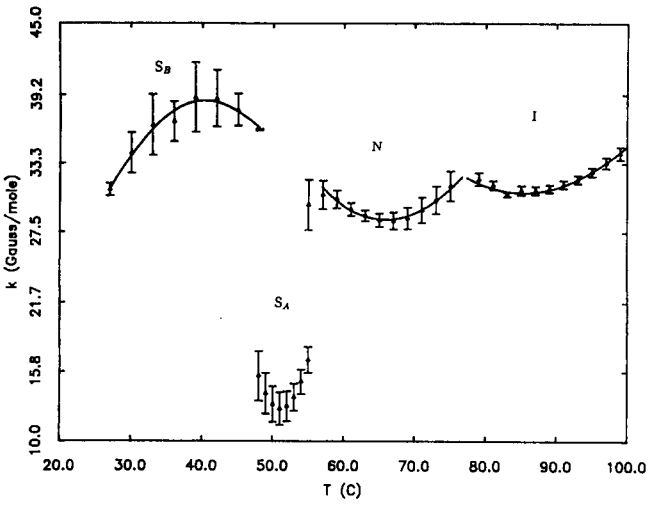

FIG. 8. The P probe in 4O,6: k vs temperature.

As noted with PD-tempone in 4O,6, the spin exchange data of *P* in the isotropic and nematic phases of 4O,6 are consistent with strong exchange. The translational diffusion constants in the isotropic phases are slightly higher than those in 6OCB–8OCB, implying faster overall probe diffusion. Rotational diffusion studies of *P* in 6OCB–8OCB[13] and *P* in 4O,6[38] have also shown $\tau_{\bar{R}}$ to be shorter in the latter. The values of $D\sim0.45\times10^{-6}$ cm^2/s obtained in the nematic and isotropic phases may be compared with the result of Cleary *et al.*[9(b)] on the closely related spin probe "octylbenzoyl spin probe", [OBSP or 2,2',6,6'-tetramethyl-4-(octyl)-benzoyl piperidine *N*-oxide] in phase V at 21 °C (nematic phase) of $D_1 = 0.48\times10^{-7}$ cm^2/s. When our results for *P* in the nematic phase of 4O,6 are extrapolated to 21 °C, we obtain $D\sim2.5\times10^{-7}$ cm^2/s, i.e., about five times faster using HE.

In the S_A phase, a significant decrease in the sensitivity of linewidth to concentration (as compared to the I and N phases) was noted at the three lower concentrations (up to 7.1 mM), but on further increasing the concentration, the linewidths were noted to increase. Such behavior, also noted for *P* in the S_A and RN phases of 6OCB–8OCB (see above), suggests a decrease in the diffusion rates that could be caused by radical solvation. As the radical concentration is increased, the solvated radicals approach each other to form aggregates, leading to an apparent "increase" in the diffusion constant as discussed below. The fact that in 4O,6 the excess linewidths increased at higher concentrations (7.1 mM), whereas no such increase in linewidth occurred in 6OCB–8OCB even at 12 mM suggests that (even though aggregation may well have occurred in the latter too) diffusion is slower in the latter. This is consistent with rotational diffusion studies of *P* in the S_A phases of 4O,6[38] and 6OCB–8OCB,[13] which show $\tau_{\bar{R}}$ to be larger in 6OCB–8OCB than in 4O,6 by about an order of magnitude, i.e., the S_A phase of

6OCB–8OCB is probably more viscous than that of 4O,6.

Some evidence to support a hypothesis involving aggregates comes from the fact that in previous HE studies in electrolytes,[3(b)] where the exchange rate was studied as a function of electrolyte concentration, the authors found that the spin exchange rate of the (uncharged) nitroxide radical DTBN decreased with increasing ionic strength of the solution and proposed that such an effect could be attributed to the formation of aggregates of radicals. The net effect of aggregation would be to reduce the frequency of bimolecular encounters leading to spin exchange, since it could be possible that only one radical of the aggregate would be involved in exchange or that aggregation may lead to a diamagnetic species. In the present context, such aggregation may occur in the densely packed S_A and RN phases. Furthermore, if the ratio of aggregates to single molecules increases with concentration in such a way that the net spin concentration increases only slightly, or if increases in radical concentration merely increases the number of groups of aggregates, the virtual constancy of ω_{HE} with concentration could be explained. It should also be noted that it is really the *activity*, not the concentration, to which the exchange rate is truly linearly proportional. Aggregation lowers the activity of the radical, thereby lowering the HE rates and also causing them to appear nonlinear in concentration.

The behavior for the excess linewidth as a function of concentration taken at all temperatures in the S_B phase was very unusual. Contrary to the usual observation, where the excess linewidth W increases fairly linearly with concentration at a given temperature, W was here observed to increase linearly for the first three concentrations (i.e., up to 7.1 mM) and then actually *decrease* at higher concentrations. (For calculating k, just the first three concentrations were used.) This is consistent with the molecules of P associating to form aggregates in the S_B phase. The initial increase in W (excess linewidth) with probe concentration is a consequence of an increased number of spins. The subsequent drop in W then suggests a tendency to aggregation (perhaps even some phase separation) at higher concentrations, thereby reducing the number of spins available for effective exchange.

VI. FURTHER DISCUSSION

A. Intermediate and weak exchange

The regime of intermediate or weak exchange corresponds to $(J_0\tau_1)^2 \ll 1$. In this case, we have [Eq. (6)]

$$\omega_{HE} = \left(\frac{N}{N-2D_M}\right)(T_2)^{-1}(\mathrm{HE}) = \tau_2^{-1}\left(\frac{J_0^2\,\tau_1^2}{1+J_0^2\,\tau_1^2}\right). \tag{21}$$

Using the expressions for τ_1 and τ_2 given by Eqs. (7a) and (4), respectively, and simplifying, we get

$$k'' \equiv \left(\frac{\sqrt{3}\gamma_e}{2}\right)\cdot\left(\frac{d(T_2^{-1}(\mathrm{HE}))}{dC}\right)^{-1} = A''\exp(\Delta E_{act}/kT) + B''\exp(E'/kT), \tag{22}$$

where

$$A'' = [7.45\times10^{14}(dD_0)]^{-1}, \tag{23a}$$

$$B'' = A''\left(\frac{36D_0^2\,J^2}{d^4}\right), \tag{23b}$$

and

$$E' = -(\Delta E_{act} - 2U(d))/R. \tag{23c}$$

In Eq. (23c), we have allowed for the dominant part of the predicted effect of the pair-correlation function on τ_1 [cf. Eq. (A4)].

The "unusual" variation of k noted for the P probe in the isotropic and nematic phases of 6OCB–8OCB and in the S_B phase of 4O,6 (see Figs. 6 and 7), may be rationalized on the basis of the assumption that as the temperature is lowered, a crossover from weak to strong exchange occurs. {We have considered a variety of mechanisms [e.g., the combination of strong exchange and significant contributions from dipolar relaxation with large (attractive or repulsive) potentials] in an effort to explain the observed maximum in the temperature variation of k with T. However, we found no other mechanisms that could account for this observation.} It can be shown, using Eqs. 4 and 7(a) in Eq. (21), that k is proportional to $1/D$ in the limit of weak exchange and to D in the strong exchange limit. Since D increases with lowering temperature, a maximum in the variation of k is expected (at $J_0^2\,\tau_1^2 \approx 1$) as the mechanism changes from weak to strong exchange. Equation (22) was used to fit our data (thereby, neglecting dipolar coupling contributions) for the two cases mentioned above. The results of such analyses are summarized in Table III.

An analysis for P in the nematic phase of 6OCB–8OCB, which considers weak exchange [Eq. (22)] gives an activation energy of 12.6 kcal/mol and a repulsive effective interaction potential $U(d)$ corresponding to 3.3 kcal/mol. Using $d = 10.46$ Å for the P probe gives $J_0 = 4.8\times10^{10}$ rad/s, while in the isotropic phase $J_0 = 1.4\times10^{11}$ rad/s, $U(d) = 4.2$ kcal/mol. A similar analysis for P in the S_B phase of 4O,6 shows the activation energy to be 11.4 kcal/mol, and a repulsive $U(d)$ of 1.9 kcal/mol. For $d = 10.46$ Å, we calculate $J_0 = 1.1\times10^{10}$ rad/s. These values of J_0 may be compared to those measured in solid nitroxides by Mao and Kreilick, who obtained $J_0 \sim 4$–8×10^{10} rad/s for DTBN and MOTA (cf. Fig. 1).[19] The analysis here has, of course, neglected any anisotropy in J. [Further evidence for a repulsive $U(d)$ is obtained in Appendix A for the cases of strong HE by comparison with the dipolar contributions.]

B. Anisotropic diffusion, orientational ordering, and Heisenberg exchange

The magnitude of the exchange interaction is roughly proportional to the square of the overlap integral (S_{AB}) for two nonorthogonal orbitals A and B being occupied by electrons[1]. Since S_{AB} depends on the mutual orientation of the two paramagnetic particles, then in the case when the exchange interaction is weak, ω_{HE} must depend on the Euler angles characterizing the mutual orientation of the particles (cf. Appendix B).

In liquid crystals, where $J(r)$ can depend on the extent of ordering of the spin radicals, the dependence of ω_{HE} on D

will be more complicated since, as shown in Appendix B, it requires an evaluation of $J(r, \Omega_1, \Omega_2)$ for the probe in the ordering field of the liquid crystal molecules. For a qualitative discussion, we may assume that the unpaired electron on the nitroxide radical resides in a $2p$ orbital of nitrogen. Atherton and Shohoji[40] have calculated the behavior of the exchange integral for a variety of canonical orientations of the interacting $2p$ orbitals. The important feature of their calculations is that $J_\sigma \gg J_\pi$ where J_σ and J_π denote the values of the exchange integral for two p orbitals exchanging via a σ and a π overlap, respectively, as shown in Fig. 9.

The molecular structures of PD-tempone and the P probe (Fig. 1) show that the ordering axes in these radicals lie along the N–O bond and are therefore perpendicular to the p-orbitals containing the electron spin. Consequently, $D_\perp$, which describes diffusion in planes normal to the lab z axis (taken as the mean director), leads to spin exchange via p-orbital overlap in which the nitroxide radicals approach each other either (i) along the interradical axis as shown in Fig. 9(a), leading to J_σ, or (ii) along directions in which the interradical axis is not normal to the director as shown in Fig. 9(b), leading to HE via J_π. Similarly, $D_\parallel$, which describes diffusion in directions parallel to the director, can lead to spin exchange via a mechanism in which the nitroxide radicals either (i) collide head-on [Fig. 9(c)] leading to J_π, or (ii) collide in a way such that the interradical axis is noncoincident with the director (Fig. 9(d)], leading to J_σ.[41] However, since as noted previously, $J_\sigma \gg J_\pi$, only those relative motions that are shown in Figs. 9(a) and 9(d) make significant contributions to J.

The influence of spin-probe ordering on J can be seen from Eqs. (B7) and (B8) in Appendix B, which also considers specific cases relevant to the different liquid crystalline phases. For the nematic phase (which has no positional ordering) with finite orientational ordering S, we obtain

$$\langle J \rangle_{nem} = (1/18) J_\sigma \, (2 + S^2), \tag{24}$$

whereas for the S_A phase, where (because of the layered structure) the interradical axes are assumed to lie perpendicular to the mean director, we obtain

$$\langle J \rangle_{sm-A} = (1/9) J_\sigma \, [1 + (1/2) S]^2. \tag{25}$$

The effect of phase transformations as the temperature of the system is lowered can be derived from Eqs. (24) and (25). For simplicity, if we consider $S = 1$ in the ordered phases, we find that across the transitions I–N–S_A, $\langle J \rangle$ changes (in units of J_σ) from (1/9) to (1/6) to (1/4). Thus, the change in J in passing from the I to N phase is comparable to that on passing from N to S_A. Therefore, while crossovers in the HE mechanism from strong to weak at the I–N transition cannot be rationalized on the basis of increased ordering alone, a large change in J with symmetry can be used to partially account for the observed changes in the HE mechanism at the N–S_A transition.

In taking proper account of the effects of temperature on the HE mechanism, the effects of τ_1 must also be considered since it is the product $(J^2\tau_1^2)$ which is the relevant quantity. From Eq. (A4), we find that $\tau_1 \sim \exp[(E_a - U(d))/kT]$, which shows that on lowering the temperature, τ_1 can either increase ($U(d) < E_a$) or de-

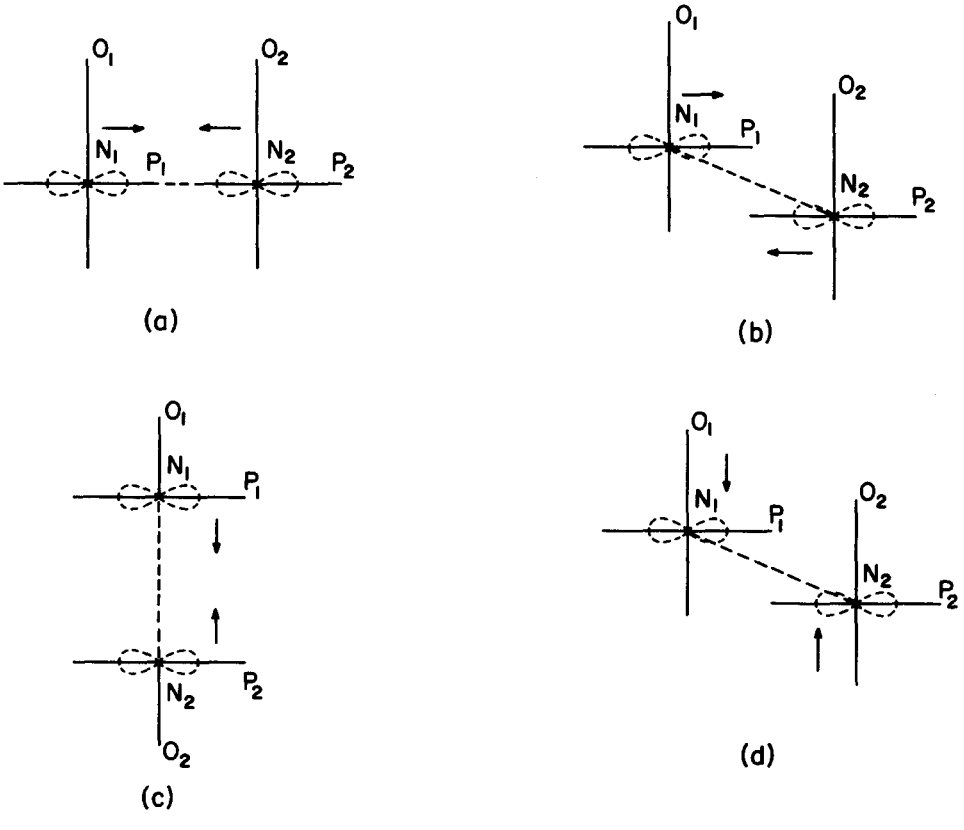

FIG. 9. Relative motion of two nitroxide radicals leading to p-orbital overlap: (a) J_σ and (b) J_π via $D_\perp$; and (c) J_π and (d) J_σ via $D_\parallel$. The interradical axis N_1N_2 is denoted by the broken lines and the direction of motion by the arrows shown at each radical.

crease ($U(d) > E_a$). Therefore, we note that while J increases with decreasing temperature in the ordered phases, the behavior of τ_1 can influence the HE mechanism in a way inconsistent with that expected from J alone. For example, the decrease in $(J_0\tau_1^2)$ at the I–N transition noted for P in 6OCB–8OCB is disfavored by J, but can be rationalized on the basis of a model which requires a somewhat decreased repulsive potential of mean force $U(d)$ in the nematic phase [in the I phase, $U(d) \approx 4.1$ kcal/mol, whereas in the nematic phase $U(d) \approx 3.3$ kcal/mol], causing τ_1 to decrease in a way such that $J_0^2\,\tau_1^2$ decreases.

The changeover from weak to strong exchange *within* a given phase (e.g., for the P probe in the N phase of 6OCB–8OCB and the S_B phase of 4O,6) is also successfully reproduced when the (repulsive) potential of mean force can cause J and τ_1 to act in opposing directions with changes in temperature. Such behavior can further be rationalized on the basis of the recent results of Shin and Freed.[42] The authors, using ESR imaging techniques, have shown that at a given temperature, the lateral diffusion constant of a spin probe [either CSL (cf. Fig. 1) or a labeled lipid] in a model membrane decreases with increased ordering of the former, and that the activation energy is proportional to S^2. Increased ordering can therefore lead to an increased activation energy E_a, thereby changing the sign of $(U(d) - E_a)$. This can effect an increase in τ_1. Furthermore, Eqs. (24) and (25) show that as ordering increases, J increases. Thus, both J and τ_1 can behave in a way such as to cause a crossover in the HE mechanism from weak to strong with decreasing temperature.

The importance of the above-described effects on $(J_0^2\,\tau_1^2)$ will increase with the anisotropy of the molecule and will thus be more for P than for PD-tempone. As a consequence, the effects of anisotropic spin exchange should be more pronounced in P than in PD-tempone (the former is also more highly ordered). The above discussion, however, considers only the effects of spin exchange. Since the relative contribution of dipolar effects goes as $(dD)^{-2}$ [Eq. (13c)], at lower temperatures where the diffusion is expected to be slower, dipolar contributions to k may gain prominence over the HE. The effects of the former could be included when the temperature range of the data permits a more reliable analysis.

VII. CONCLUSIONS AND SUMMARY

Our results with PD-tempone and the P probe in the two liquid crystal solvents (4O,6 and 6OCB–8OCB) show that while the concentration-dependent relaxation may be adequately described in terms of strong exchange for the former, the latter (P probe) most likely exhibits weak exchange in 6OCB–8OCB and in the S_B phase of 4O,6. This difference in behavior between the two spin probes has been discussed in terms of the higher anisotropy and orientational ordering (in the mesophases) of the P probe compared to PD-tempone.

With PD-tempone, k varies rather smoothly across the N, S_A, and RN phases in the cyanobiphenyls 6OCB–8OCB and no discontinuities in the activation energies are observed. On the other hand, k shows abrupt discontinuities across the N, S_A, and S_B phases for PD-tempone in 4O,6, which forms monolayered smectics. Given the hypothesis that the formation of smectic layers is accompanied by probe expulsion,[14] it is concluded that while in 6OCB–8OCB probe expulsion occurs *prior* to the formation of the S_A phase, such expulsion in 4O,6 occurs *following* the N–S_A transition in the S_A phase, in agreement with previous studies on ordering and rotational dynamics.[14] Furthermore, the fact that in 6OCB–8OCB the transitions leading to the RN phase do not show discontinuities in E_{act} supports the belief[13] that no dramatic structural changes occur during nematic reentrance.

The P probe shows strong exchange in the isotropic phases of 4O,6. However, in the isotropic phase of 6OCB–8OCB and in the ordered phases, a tendency toward weak exchange is noted. In the S_A phases of both 4O,6 and 6OCB–8OCB, no increase in excess linewidth was noted to occur till high concentrations of P were reached (7.1 mM in 4O,6, and in 6OCB–8OCB, even at 12 mM no change was detected). Such behavior for the P probe can be rationalized on the basis of the assumption that in the S_A phases the diffusion rate of P is considerably reduced. This reduction in the apparent value of D may be caused by solvent structure around the probe molecules; as a result, diffusion involving a species with a larger effective mass now occurs. The fact that at higher concentrations HE begins to occur (at least in 4O,6) suggests that with increasing concentration, the solvated probe molecules tend to aggregate, thereby leading to an apparent increase in D as measured by HE. As noted below, the solvation shell surrounding each probe molecule, which prevents the radicals from approaching each other at distances equal to the sum of their van der Waals radii, provides a convenient model for explaining the repulsive potential of mean force $U(d)$ that was calculated for P. An alternative that we have not explored, would be to consider the effects of hydrodynamic flows as solute molecules try to approach each other.[43,44]

The unusual temperature variation of k observed with the P-probe in the I and N phases of 6OCB–8OCB and the S_B phase of 4O,6 may result from a repulsive potential $U(d)$, which can cause τ_1 to either increase ($U(d) < \Delta E_{act}$) or decrease ($U(d) > \Delta E_{act}$) as the temperature is lowered. Thus, even though $\langle J \rangle$ increases with ordering (i.e., with decreasing temperature), a more significant *decrease* in τ_1 could cause $(J_0\tau_1)^2$ to decrease.

In general, we note that our fits of k vs T to a sum of the two exponentials describing the HE and dipolar contributions to the excess linewidth are reasonable. We find that (with the exception of PD-tempone in 6OCB–8OCB) the relative contributions of the two effects are dependent upon the phase of the liquid crystalline solvent (see Table II). The diffusion constants that we estimate from the fits are about $4—8\times10^{-7}$ cm^2/s for P in the I and N phases, and $0.8–1.9\times10^{-6}$ cm^2/s for PD-tempone in the various phases studied. These diffusion rates are somewhat higher than those that have been measured using ESR imaging techniques,[9] but become more comparable when extrapolated to the temperatures at which the imaging data were collected. In making such comparisons, however, it must be noted that

the diffusion coefficients obtained from HE measurements are model dependent and require a knowledge of the encounter distance. For weak exchange, the exchange integral and the effective potential of mean force $U(d)$ are additional quantities that are used as fitting parameters. In cases involving weak exchange, we find that $U(r)$ at $r = d$ is repulsive, suggesting the possibility of a solvation sphere surrounding the probe that prevents the probes from getting any closer to each other than the sum of their solvated radii. The value of J typically obtained from these fits lies between 1.1×10^{10} rad/s (P in the S_B phase of 4O,6) and 1.4×10^{11} rad/s (P in the I phase of 6OCB–8OCB). In cases involving strong exchange, our comparisons of D obtained from HE contributions vs those obtained from dipolar contributions are also consistent with the need to include a repulsive $U(d)$.

In the cases that involve weak exchange, one expects dipolar contributions to make more significant contributions to the excess linewidth as compared to the strong exchange cases. Though we were aware of this, we were unable to include dipolar corrections in our fits to the data since a separation of HE and dipolar contributions could not easily be made, and also involved more fitting parameters than the availability (and quality) of experimental data could justify. The newly developed two-dimensional Fourier-transform electron–electron double resonance (2D-FT-ELDOR) technique[29(c),45] provides a useful method of resolving the dipolar and HE contributions, when used in conjunction with the homogeneous linewidth measurement from the electron spin echo (ESE) technique. For example, $\Delta M_I = \pm 1$ crosspeak volumes yield $(\omega_{HE} + \omega_{EED})$[29] directly, while the concentration-dependent homogeneous linewidth may then be decomposed to assess the dipolar and HE contributions. Clearly, such experiments are needed in order to allow an unambiguous separation of these relaxation mechanisms and thereby extricate the "microscopic" translational diffusion coefficient for P probe in liquid crystals more reliably.

ACKNOWLEDGMENTS

Supported by NSF Grants No. DMR 89-01718 and No. CHE 8703014 and NIH Grant No. GM-25862.

APPENDIX A: THE EFFECT OF INTERACTION POTENTIALS AND PAIR CORRELATION FUNCTIONS

Pedersen and Freed (PF)[18] have provided a more general formulation for Heisenberg spin exchange than the earlier work of Eastman *et al.*[3] on which the analysis described in Sec. V was based. The former supplants the earlier theory by: (i) allowing for the finite range of the exchange interaction in the expression for τ_1, the lifetime of the exchanging radical pair; (ii) taking account of the interaction potential between radicals and of the liquid structure via the pair-distribution function; and (iii) allowing for the successive reencounters of the same radical pair after they have separated (i.e., the cage effect in liquids). Here we emphasize the effect of pair-correlation functions in the analysis of some data which could not be rationalized on the basis of the simple treatment.[43]

The results of the Pedersen–Freed treatment may be summarized by writing the HE frequency as

$$\omega_{HE} = \left(\frac{N}{N-2D_M}\right)(T_2)^{-1}(HE)$$
$$= 4\pi dD\mathcal{N}g(J_0d^2/D,\lambda d)p(d_t), \quad \text{(A1)}$$

where the symbols have their usual meanings [cf. Eq. (12)]; g and p in Eq. (A1) are defined by

$$g(J_0d^2/D,\lambda d) \approx f^* + (\lambda d)^{-1}\ln\left[\left(\frac{J_0d^2}{4D}\right)\cdot\frac{f^*}{\lambda d}+1\right], \quad \text{(A2)}$$

$$p(d_t) \approx \frac{(J_0\tau_1)^2}{1+(J_0\tau_1)^2}, \quad \text{(A3)}$$

$$\tau_1 \approx \left(\frac{d^2}{2D(\lambda d)}\right)[1+(\lambda d)^{-1}]\,(f^*)^{-1}\exp[-U(d)/kT], \quad \text{(A4)}$$

and f^* is a "partition function" given by

$$(f^*)^{-1} = d\int_d^\infty \frac{\exp(U(r)/kT)}{r^2}\,dr. \quad \text{(A5)}$$

In these equations, λ is related to the finite range of the encounter leading to spin exchange [see Eq. (7b)] and $U(r)$, the potential of mean force, is related to the pair-correlation function $g(r)$ by

$$\ln g(r) \equiv -U(r)/kT. \quad \text{(A6)}$$

(Note also that J_0 in Ref. 18 is one-half the J_0 used in this work and D in Ref. 18 is twice the D used in this work.)

We shall now simplify Eq. (A1) to obtain an approximate, but useful form for $T_2^{-1}(HE)$. For typical values [of nitroxides[4,46] of J_0 (10^{11}–10^{12} rad/s), d($\sim$7 Å) and D in liquid crystals (10^{-6}–10^{-7} cm^2/s), the logarithmic term in Eq. (A2), which approximates the correction to τ_2^{-1} in Eq. (4) due to the finite range of $J(r)$, may be neglected in comparison to f^*. Equation (A1) then simplifies to

$$\left(\frac{N}{N-2D_M}\right)T_2^{-1}(HE)$$
$$= 4\pi dD(10^{-3}N_A)Cf^*\cdot\frac{(J_0\tau_1)^2}{1+(J_0\tau_1)^2}, \quad \text{(A7a)}$$

which, in the limit of strong exchange, becomes

$$\left(\frac{N}{N-2D_M}\right)T_2^{-1}(HE) = 4\pi dD(10^{-3}N_A)Cf^*. \quad \text{(A7b)}$$

It has also been suggested[23] that the effect of pair-correlation functions on the electron-spin dipolar interactions is to replace $J(0)$ in the expression for T_2^{-1} (dip) [Eq. (11)] by $(f^*)^{-1}\exp(-U(d)/kT)J(0)$. With this substitution, Eq. (11) now becomes

$$T_2^{-1}(dip) \approx \hbar^2\gamma_e^4 S(S+1)\left(\frac{5N+8D_M}{24N}\right)\cdot\frac{48\pi}{15}\cdot\frac{4(10^{-3}N_AC)}{27dD}\times[f^*\exp(U(d)/kT)]^{-1}. \quad \text{(A8)}$$

Using Eqs. (A7b) and (A8), and the Stokes–Einstein expression for the diffusion coefficient [Eq. (5)], it can be shown that

$$k = \frac{dW}{dC}$$
$$\equiv \left(\frac{2}{\sqrt{3}\gamma_e}\right) \cdot \frac{d(T_2^{-1}(\mathrm{HE}) + T_2^{-1}(\mathrm{dip}))}{dC}$$
$$= A''f^*\left(\frac{T}{\eta}\right) + B''[f^* \exp(U(d)/kT)]^{-1}\left(\frac{\eta}{T}\right), \tag{A9}$$

where

$$A'' \approx 4.85 \times 10^{-3} \tag{A9a}$$

and

$$B'' \approx 8.48 \times 10^{4}. \tag{A9b}$$

Alternatively, one may substitute the Arrhenius expression for D into Eqs. (A7) and (A8) [as in Eq. (19)] to obtain

$$k = \left(\frac{2}{\sqrt{3}\,\gamma_e}\right) \cdot \frac{d(T_2^{-1}(\mathrm{HE}) + T_2^{-1}(\mathrm{dip}))}{dC}$$
$$= A'f^* e^{(-E_{\mathrm{act}}/kT)} + B'[f^* e^{(U(d)/kT}]^{-1} e^{(E_{\mathrm{act}}/kT)}, \tag{A10}$$

where A' and B' in Eq. (A10) have the same values as the A and B given by Eq. (20). In Eqs. (A9) and (A10), f^* is temperature dependent [see Eq. (A5)].

The use of Eq. (A9) for strong exchange is illustrated with an example. Berner and Kivelson[4] have measured k as a function of T/η for ditertiary butyl nitroxide (DTBN) in several isotropic liquids. Their data for perdeuterated DTBN in ethylene glycol and water are shown by the open circles in Figs. 10(a) and 10(b). Attempts at fitting the experimental curve using the simpler expression 19(b) [or its (η/T) analog] were unsuccessful, and seemed to require the *ad hoc* assumption that the hydrodynamic radius d appearing in the expressions for HE and dipolar relaxation [Eqs. (11) and (12)] was: (i) different in the two cases [i.e., $d(\mathrm{dip}) \neq d(HE)$]; and that (ii) the ratio $d(\mathrm{dip})/d(\mathrm{HE})$ was temperature dependent. Equation (A9) provides an explanation in that the apparent "inequality" and "temperature dependence" of d is a consequence of the fact that the supposed constant factors A and B in Eq. (19) are not really temperature independent, but implicitly depend on temperature (and in different ways) through f^* and $\exp(U(d)/kT)$ according to Eq. (A9). If f^* is assumed, for convenience in data fitting, to obey a simple power law expression in (T/η) of the form

$$f^* \sim a(T/\eta)^m, \tag{A11}$$

then an expression for dW/dC of the form

$$\frac{dW}{dC} = aA''\left(\frac{T}{\eta}\right)^{(m+1)} + aB'' \exp(-U(d)/kT)\left(\frac{T}{\eta}\right)^{-(m+1)} \tag{A12}$$

can be used to fit the Berner–Kivelson results.[4] The results of such an analysis, plotted as the solid line through the open circles in Fig. 10, yield $m = -0.075$, $a = 1.50$, and $U(d) = (7.0 \pm 0.6)$ kcal/mol. Thus, a weak variation for f^* with temperature is indicated (Fig. 11) as expected,[18] and a large effective repulsive potential of mean force at $r = d$ (RT at room temperature is about 0.6 kcal/mol). The values of f^* in the (T/η) range studied by Berner and Kivelson are close to unity, lying between 1.1 and 0.7, as shown by the solid circles in Fig. 11. The values of f^* that are less than unity are consistent with a repulsive pair-correlation function, whereas $f^* > 1$ [which is observed at the two low (T/η) data points in Fig. 10] are consistent with attraction between the radicals. At these lower temperatures, therefore, it is proposed that while $U(d) > 0$, $U(r)$ varies in a way such that the integrated area in Eq. (A5) [which is a measure of $(f^*)^{-1}$] is overall negative. The effective repulsive potential of mean force would suggest that surrounding each radical there is a large solvation sphere which prevents the radicals from approaching each other at distances shorter than the sum of

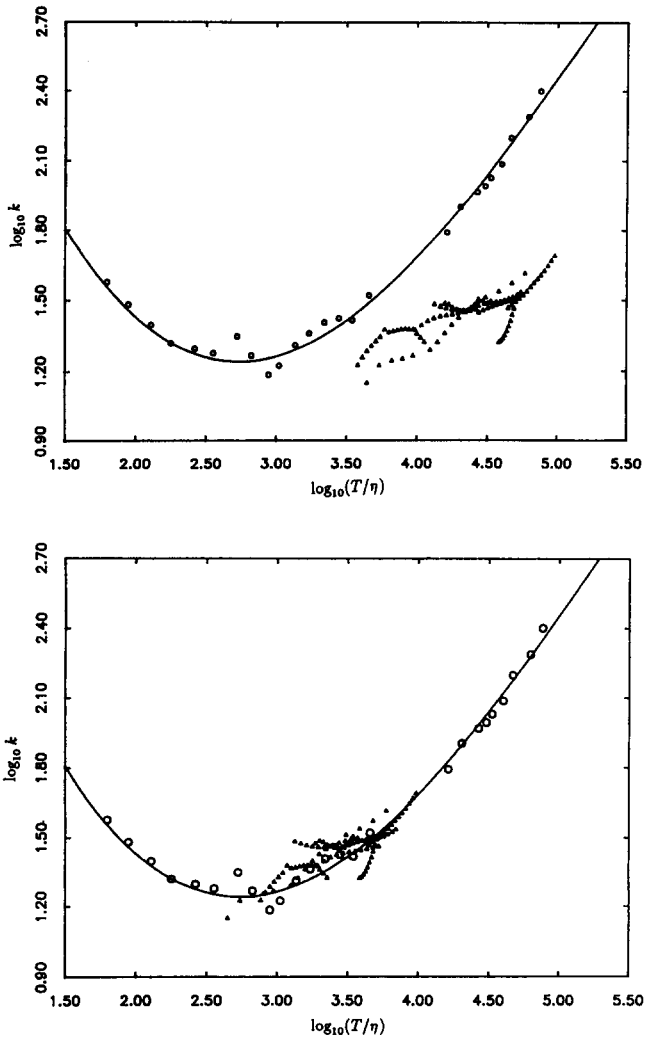

FIG. 10. $\log_{10} k$ vs $\log_{10}(T/\eta)$ for DTBN in water and ethylene glycol; data taken from Berner and Kivelson (Ref. 4). The curve through the data (solid line) represents our best fit using Eq. (A12), which includes the effect of an interaction potential. Also shown are our data plotted on the same scale, using (a) $\kappa = 1$ and (b) $\kappa = 0.1$ for PD-tempone in 4O,6 and 6OCB–8OCB; $\kappa = 0.2$ and 0.13 for the P: probe in 4O,6 and 6OCB–8OCB, respectively.

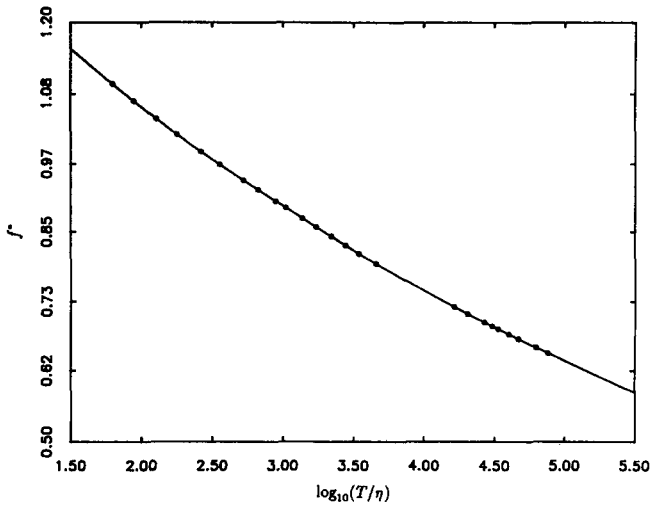

FIG. 11. Variation of f^* with temperature for the fit shown in Fig. 9: $f^* = 1.50(T/\eta)^{-0.075}$. The dots represent the values of f^* calculated for the Berner–Kivelson data.

the radii of the solvated species. [Since the effects of $\exp(-U(d)/kT)$ are more pronounced than those of f^*,[18] only the former was used in the weak exchange fits in Sec. VI A.]

We have also performed numerical simulations to assess the role of pair-correlation functions using the following exponentially damped sinusoidal form for $g(r)$:

$$g(r) = 1 + Ae^{-\zeta(r-d)}\cos(2\pi r/d). \qquad \text{(A13)}$$

In Eq. (A13), ζ measures the range of static correlations and A is the amplitude of modulation of the number density of particles.[47] The large value for $U(d)/kT$ for the Berner–Kivelson data (about 12) implies that A is close to -1.0. From Eqs. (A5) and (A6), we have

$$(f^*)^{-1} = d\int_d^\infty \frac{1}{g(r)r^2}\,dr. \qquad \text{(A14)}$$

The experimentally observed values of f^* lying in the range 0.7–1.0 are obtained when $\zeta > 1.0$, while the values of f^* larger than 1.0 (i.e., attractive) could not be reproduced using the $g(r)$ in Eq. (A13). A possible explanation may be that this $g(r)$ does not adequately describe the pair correlation over the entire temperature range (both ethylene glycol and water form hydrogen bonds, and the extent of association changes with temperature, thus affecting the solvent properties).

Also shown in Figs. 10(a) and 10(b) (solid triangles) are our data for T/η calculated using the values of the mean rotational correlation times $\tau_{\bar{R}}$ for the systems studied here.[13,14,38] In Fig. 10(a) the calculations of T/η were performed using $\kappa = 1$ [cf. Eq. (10)] whereas in Fig. 10(b), κ was adjusted in such a way as to shift our T/η values to coincide with the Berner–Kivelson data. The values of κ for the two spin probes that were consistent with these shifts are as follows: (i) PD-tempone in 40,6 and in 60CB–80CB, $\kappa = 0.10$; (ii) P probe in 40,6, $\kappa = 0.20$; P probe in 60CB–80CB, $\kappa = 0.13$. Such values of κ are fairly typical of what were noted earlier for PD-tempone in a variety of solvents.[48] As expected for a larger spin probe, which is structurally more like the liquid crystal solvents (i.e., P probe), κ is larger than PD-tempone.

The relatively flat region in Fig. 10 [lying between $10^2 < (T/\eta) < 10^4$] is the region where k is least sensitive to changes in (T/η). Therefore, data restricted to this region would not be expected to yield reliable estimates of the fitting parameters of Eq. (A12). Our own data show the same relatively flat behavior as that seen between $10^2 < (T/\eta) < 10^4$ for the isotropic solvents. Therefore, it is not surprising that parameters estimated using either Eq. (A12) or Eq. (19b) (cf. Table I) are associated with large errors, particularly in those phases which have a narrow temperature range. Nevertheless, we do find that our data exhibit the same trends as we have just discussed for the Berner–Kivelson results. In fact, the discrepancy between the estimates of D from the HE vs the dipolar contributions noted in Sec. IV B can be interpreted as due to an effective repulsive $U(d) \sim 1$–4 kcal/mol.

APPENDIX B: ANISOTROPIC EFFECTS IN SPIN EXCHANGE

Consider a Cartesian coordinate system, shown in Fig. 12(a), where the z axis lies along the interradical axis connecting the nitrogen atoms N_1 and N_2 of the two nitroxide radicals N_1–O_1 and N_2–O_2. For simplicity, each N–O bond is assumed to lie along the symmetry axis of the molecule containing the bond. Let (θ_i', ϕ_i') be the polar coordinates of the p-orbitals N_i–P_i centered on N_i. (Note that N_i–O_i is

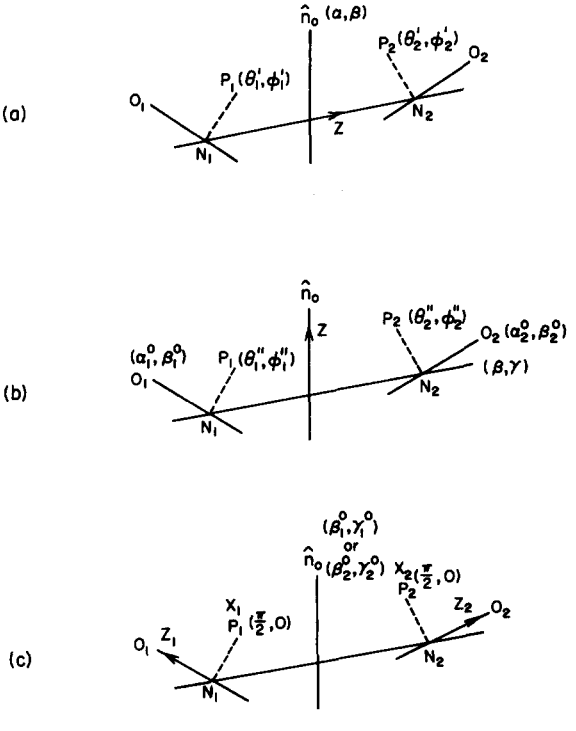

FIG. 12. Relative orientations of two nitroxide radicals N_1O_1 and N_2O_2 in different Cartesian coordinate systems as discussed in the text. The p-orbitals lie along N_1–P_1 and N_2–P_2. In each case, the z axis of the coordinate system is indicated by an arrow, and the polar coordinates of the relevant vectors are shown in that coordinate frame. (a) The internuclear system; (b) the lab system; (c) the molecular systems.

perpendicular to N_i–P_i.) We shall assume that J_σ, which represents the exchange integral when the two orbitals N_1–P_1 and N_2–P_2 overlap along the interradical axis (see Fig. 9), is by far the dominant term contributing to J, and that contributions due to J_π may be neglected.[40] With this approximation, we shall write

$$J = J_\sigma \cos\theta_1' \cos\theta_2' [\cos\theta_1' \cos\theta_2' + \sin\theta_1' \sin\theta_2' \cos(\phi_1' - \phi_2')] \quad \text{(B1)}$$

which is a relatively simple expression yielding the expected angular dependence of J. [Eq. (B1) is the same as Eq. (9a)].

We now consider the effect upon J of (rapid) rotations about the axes N_i–O_i (θ_i,ϕ_i), i.e., the symmetry axes of the molecules. The effect of rotational transformations on J is simplified on expressing the latter in terms of spherical harmonics according to

$$J = \frac{4\pi}{3} J_\sigma \left(\tfrac{1}{3}A - \tfrac{1}{5}B\right) \quad \text{(B2)}$$

where

$$A = (4/5) Y_{2,0}(\theta_1',\phi_1') Y_{2,0}(\theta_2',\phi_2') + (1/\sqrt{5\pi}) \times [Y_{2,0}(\theta_1' + \phi_1') + Y_{2,0}(\theta_2',\phi_2')] + (1/4\pi) \quad \text{(B3a)}$$

and

$$B = Y_{2,1}(\theta_1',\phi_1') Y_{2,-1}(\theta_2',\phi_2') + Y_{2,-1}(\theta_1',\phi_1') Y_{2,1}(\theta_2',\phi_2'). \quad \text{(B3b)}$$

[Note that Eq. (B1) was chosen in part to allow this simple decomposition into spherical harmonics.] We shall now express J in a laboratory fixed frame, so that the anisotropy of J can be expressed in terms of variables that describe the ordering of the probe molecules. This transformation is achieved in two steps: (i) a transformation from the "internuclear frame" (abbreviated as int), defined such that its z axis lies along the internuclear axis N_1–N_2 and its x axis lies in the plane containing the N_1–O_1 bond, to the lab frame (lab), defined such that its z axis lies parallel to the mean director. The Euler angles for this transformation are (α,β,γ). (ii) A transformation from the laboratory frame to the molecular frame (mol), defined as having its z axis along the N_i–O_i bond, and its x axis along the p orbital N_i–P_i. The appropriate Euler angles are $(\alpha_i^0\beta_i^0\gamma_i^0)$. These coordinate frames are shown in Figs. 12(a)–12(c). With these definitions, we have[49]

$$Y_{2,m}^{\text{int}}(\theta_i',\phi_i') = \sum_{m'} Y_{2,m'}^{\text{lab}}(\theta_i'',\phi_i'') \mathscr{D}_{m'm}^2(\alpha,\beta,\gamma)_{(\text{lab}\to\text{int})} = \sum_{m'}\sum_{m''} Y_{2,m''}^{\text{mol}}(\theta_i^m,\phi_i^m) \mathscr{D}_{m''m'}^2(\alpha_i^0\beta_i^0\gamma_i^0)_{(\text{mol}\to\text{lab})} \times \mathscr{D}_{m'm}^2(\alpha,\beta,\gamma)_{(\text{lab}\to\text{int})}. \quad \text{(B4)}$$

In these equations (θ_i'',ϕ_i'') and (θ_i^m,ϕ_i^m) are the polar coordinates of the orbital N_i–P_i in the laboratory and molecular frames, respectively. Note that since in the latter frame, the x_i axes are chosen to lie along the N_i–P_i direction, it follows that $(\theta_i^m,\phi_i^m) \equiv (\pi/2,0)$. Also, (β,γ) denote the polar coordinates of the internuclear vector in the director (i.e., lab) frame, and $(\alpha_i^0\beta_i^0)$ are the coordinates of the N_i–O_i vector in the laboratory fixed frame (also see Fig. 12).

The rotational dynamics of each molecule leads to a time dependence of the angles $(\alpha_i^0\beta_i^0\gamma_i^0)$. If we assume that the rotational motion is fast compared to the duration of the exchange interaction (cf. Sec. II A), then it is appropriate to average $\mathscr{D}_{m''m'}^2(\alpha_i^0\beta_i^0\gamma_i^0)$ in Eq. (B4) over this rotational motion. For uniaxial liquid crystals, the well-known result of such averaging is[30]

$$\langle \mathscr{D}_{m''m'}^2(\alpha_i^0\beta_i^0\gamma_i^0)\rangle = \langle \mathscr{D}_{m'',0}^2(\alpha_i^0\beta_i^0\gamma_i^0)\rangle \delta_{m',0}. \quad \text{(B5a)}$$

For convenience, let us consider axially symmetric ordering of the nitroxide molecule, then[30]

$$\langle \mathscr{D}_{m'',0}^2(\alpha_i^0\beta_i^0\gamma_i^0)\rangle = S\delta_{m'',0}. \quad \text{(B5b)}$$

where S is the order parameter. This substitution leads to

$$Y_{2,m}^{(\text{int})}(\theta_i',\phi_i') = Y_{2,0}^{\text{mol}}(\pi/2) S \mathscr{D}_{0,m}^2(\beta,\gamma)_{(\text{lab}\to\text{int})} = -(S/2) Y_{2,m}(\beta,\gamma) \quad \text{(B6)}$$

where on the right-hand side, the subscript (lab→int) is implicit. Equation (B6), when substituted into Eqs. (B2) and (B3) leads to

$$\langle J\rangle = \frac{4\pi}{3} J_\sigma \left(\tfrac{1}{3}A' - \tfrac{1}{5}B'\right), \quad \text{(B7)}$$

where

$$A' = \left(\frac{1}{4\pi}\right) [\tfrac{1}{2}S(3\cos^2\beta - 1) - 1]^2 \quad \text{(B8a)}$$

and

$$B' = -\frac{15}{16\pi} S^2 \sin^2\beta \cos^2\beta, \quad \text{(B8b)}$$

We shall now consider some limiting cases of Eq. (B7) that are useful in understanding our results described in Sec. V.

(i) $S = 0$: This is the case of an isotropic liquid, and leads to the result

$$\langle J\rangle_{S=0} = (1/9) J_\sigma. \quad \text{(B9)}$$

(ii) $S = 1$: The molecules are perfectly ordered. In this case, we have

$$\langle J\rangle_{S=1} = (1/4) J_\sigma \sin^2\beta. \quad \text{(B10)}$$

According to Eq. (B10) [as well as Eq. (B7)] the "effective" exchange interaction depends upon the angle β, i.e., there will be a range of $\langle J\rangle$ depending on the orientation of the internuclear axis with respect to the nematic director for each collision. For example, Eq. (B10) shows that when the radicals diffuse towards each other along an axis which is perpendicular to the mean director [i.e., $\beta = 90°$, see Fig. 9(a)], $\langle J\rangle$ is at its maximum value $(1/4)J_\sigma$. However, when the interradical axis lies along the nematic director [i.e., $\beta = 0°$ or 180°, see Fig. 9(b)], $\langle J\rangle = 0$.

Now for convenience, let us average over $\sin^2\beta$ in Eq. (B10) to describe an "average collision." Thus, for example, in the nematic phase, the interradical axis is randomly oriented with respect to the director, so that

$$\langle \sin^2\beta\rangle = \frac{\int_0^\pi \sin^3\beta\, d\beta}{\int_0^\pi \sin\beta\, d\beta} = (2/3).$$

In the S_A phase, the molecules are arranged in layers with the principal diffusion being lateral diffusion in the smectic plane, so that the distribution function is peaked about $\beta = 90°$; in this case,

$$\langle \sin^2 \beta \rangle \cong \frac{\int_0^\pi \sin^3 \beta \delta [\beta - (\pi/2)] \, d\beta}{\int_0^\pi \sin \beta \, \delta [\beta - (\pi/2)] \, d\beta} = 1.$$

Therefore, when the liquid crystalline system is cooled from the N to the S_A phase, the average exchange integral for a moderately ordered spin probe could increase.[50]

[1]Yu. N. Molin, K. M. Salikhov, and K. I. Zamaraev, *Spin Exchange* (Springer, Berlin, 1980).

[2](a) J. H. Freed, J. Chem. Phys. **45**, 3452 (1966); (b) J. Phys. Chem. **71**, 38 (1967); (c) W. Plachy and D. Kivelson, J. Chem. Phys. **47**, 3312 (1967); (d) A. E. Stillman and R. N. Schwartz, J. Magnetic Reson. **22**, 269 (1976).

[3](a) M. P. Eastman, R. G. Kooser, M. R. Das, and J. H. Freed, J. Chem. Phys. **51**, 2690 (1969); (b) M. P. Eastman, G. V. Bruno, and J. H. Freed, *ibid.* **52**, 2511 (1970); (c) J. C. Lang and J. H. Freed, *ibid.* **56**, 4103 (1972).

[4]B. Berner and D. Kivelson, J. Phys. Chem. **83**, 1406 (1979).

[5](a) B. L. Bales, J. A. Swenson, and R. N. Schwartz, Mol. Phys. **28**, 143 (1974); (b) L. L. Jones and R. N. Schwartz, Mol. Phys. **43**, 527 (1981).

[6]J. Sachse, M. D. King, and D. Marsh, J. Magnetic Reson. **71**, 385 (1987).

[7]W. L. C. Vaz, R. M. Clegg, and D. Hallmann, Biochemistry **24**, 781 (1985).

[8]M. E. Moseley and A. Loewenstein, Mol. Cryst. Liq. Cryst. **90**, 117 (1982).

[9](a) J. P. Hornak, J. K. Moscicki, D. J. Schneider, and J. H. Freed, J. Chem. Phys. **84**, 3387 (1986); (b) D. A. Cleary, Y.-K. Shin, D. J. Schneider, and J. H. Freed, J. Magnetic Reson. **79**, 474 (1988); (c) J. K. Moscicki, Y.-K. Shin, and J. H. Freed, J. Magnetic Reson. **84**, 554 (1989).

[10]J. H. Freed, J. Chem. Phys. **66**, 4183 (1977).

[11]S. A. Zager and J. H. Freed, Chem. Phys. Lett. **109**, 270 (1984).

[12]P. E. Cladis, Mol. Cryst. Liq. Cryst. **67**, 177 (1981).

[13]A. Nayeem and J. H. Freed, J. Phys. Chem. **93**, 6359 (1989).

[14]W. J. Lin and J. H. Freed, J. Phys. Chem. **83**, 379 (1979).

[15]Conversely, the "fast exchange" condition, which occurs when the three N hyperfine lines merge together, is given by $\omega_{HE} \gg \gamma_e a_N$. One speaks of "moderate exchange" when $\omega_{HE} \approx \gamma_e a_N$, which is obtained when the lines start merging.

[16]J. Frenkel, *Kinetic Theory of Liquids* (Dover, New York, 1956).

[17]This is the conventional form for the lifetime of "reacting pairs." It is based upon rewriting $(\tau_1^c)^{-1} \simeq 4\pi D d / \Delta V$, where ΔV is the "reaction volume." Early theories arbitrarily defined ΔV as the total volume swept by the interacting pair, i.e., $(4/3)\pi d^3$, but detailed studies (Ref. 17) have shown that $\Delta V \simeq 4\pi d^2 \Delta r_J$, which is the annular volume of the contact region, i.e., $J(r)$ equals J_0 from d to $d + \Delta r_J$, and is zero otherwise. This yields $\tau_1^c = d\Delta r_J / D$.

[18](a) J. H. Freed and J. B. Pedersen, Adv. Magn. Reson. **8**, 1 (1976); (b) J. H. Freed in *Chemically Induced Magnetic Polarization*, edited by L. T. Muus, P. W. Atkins, K. A. Mc Lauchlan, and J. B. Pedersen (Reidel, Dordrecht, 1977).

[19](a) C. R. Mao and R. W. Kreilick, Chem. Phys. Lett. **34**, 363 (1975); (b) Mol. Phys. **31**, 1447 (1976).

[20]G. P. Zientara and J. H. Freed, J. Phys. Chem. **83**, 3333 (1979).

[21]K. S. Chu, N. K. Ailawadi, and D. S. Moroi, Mol. Cryst. Liq. Cryst. **38**, 45 (1977).

[22]A. Abragam, *The Principles of Nuclear Magnetism* (Oxford University, Oxford, 1961).

[23]L. P. Hwang and J. H. Freed, J. Chem. Phys. **63**, 4017 (1975).

[24]A. Belorizky and A. Gallice, J. Phys. (Paris) **36**, 991 (1975).

[25]J. S. Hwang, R. P. Mason, L. P. Hwang, and J. H. Freed, J. Phys. Chem. **79**, 489 (1975).

[26]J. A. Murphy, J. W. Doane, Y. Y. Hsu, and D. L. Fishel, Mol. Cryst. Liq. Cryst. **22**, 133 (1973).

[27]R. N. Schwartz, L. L. Jones, and M. K. Bowman, J. Phys. Chem. **83**, 3429 (1979).

[28]S. A. Zager and J. H. Freed (unpublished results). When the β deuterons in PD-tempone were replaced by protons, the intrinsic widths obtained by deconvoluting the observed (envelope) lines did not differ much from the previous values.

[29]The pseudosecular terms of the dipolar interaction (i.e., terms in $S_{1\pm} S_{2\mp}$) will also play a role equivalent to ω_{HE} in Eq. (15). Therefore, more rigorously, ω_{HE} in Eq. (15) should be replaced by $\omega_{EX} = \omega_{HE} + \omega_{EED}$, where ω_{EED} is the pseudosecular dipolar contribution. However, since in the present work, $T_2^{-1}(\text{dip})/T_2^{-1}(\text{HE}) < 1$ and $\omega_{EED} = (3/19) T_2^{-1}(\text{dip})$, this is not a significant correction [see (a) J. H. Freed in *Multiple Electron Resonance Spectroscopy*, edited by M. Dorio and J. H. Freed (Plenum, New York, 1979), Chap. 3; (b) Ref. 46; (c) J. Gorcester and J. H. Freed, J. Chem. Phys. **88**, 4678 (1988), Ref. 49.]

[30]C. F. Polnaszek and J. H. Freed, J. Chem. Phys. **79**, 2283 (1975).

[31](a) P. R. Bevington, *Data Reduction and Error Analysis in the Physical Sciences* (McGraw-Hill, New York 1969); (b) W. H. Press, B. P. Flannery, S. A. Teukolsky, and W. T. Vetterling, *Numerical Recipes: The Art of Scientific Computing* (Cambridge University, New York, 1986).

[32]In some cases, the set of parameters that gave the lowest value of χ^2 had to be rejected on either one of two grounds: (i) the parameters did not make any physical sense, e.g., the value of B in Eq. (19b) came out to be negative; or (ii) the value of D calculated from B was five to ten times higher than that calculated from A. Therefore, a set of parameters that did not necessarily yield the lowest χ^2, but a χ^2 not very different from the lowest (i.e., within a factor of 2) and which was physically more acceptable, was used.

[33]Using a common set of parameters for fitting the data in the N, S_A, and RN phases did not yield the lowest χ^2 in this case. In fact, a better fit to the S_A and RN phases (i.e., using a common set of parameters for only these phases) was obtained using a weak exchange model; but then the fits to the N and I phases (or the N and I phases individually) converged to a χ^2 minimum at which B (the dipolar contribution) was negative. This therefore had to be rejected because the results were then physically untenable.

[34]A. J. Leadbetter, F. P. Temme, A. Heidemann, and W. Howells, Chem. Phys. Lett. **34**, 363 (1975).

[35]M. K. Ahn, J. Magnetic Reson. **22**, 289 (1976).

[36]G. J. Kruger, Phys. Rep. **82**, 229 (1982).

[37]G. P. Zientara and J. H. Freed, J. Chem. Phys. **71**, 3861 (1979).

[38]E. Meirovitch, D. Igner, E. Igner, G. Moro, and J. H. Freed, J. Chem. Phys. **77**, 3915 (1982).

[39]F. Noack, Mol. Cryst. Liq. Cryst. **113**, 247 (1984).

[40]N. M. Atherton and M. C. B. Shohoji, J. Chem. Soc. Faraday Trans. **79**, 1243 (1983).

[41]The four cases shown in Fig. 9, of course, represent idealized situations in which perfect ordering of the N–O radicals is assumed, and molecular rotation about N–O, which causes the p orbitals to change their relative orientation during the collision (which leads to σ–π mixing) is ignored. These matters are considered in Appendix B.

[42]Y.-K. Shin and J. H. Freed, Biophys. J. **55**, 537 (1989).

[43]These corrections are related to equilibrium properties of the fluids. Additional corrections due to hydrodynamic flow discussed by PF [J. B. Pedersen and J. H. Freed, J. Chem. Phys. **62**, 1790 (1975)] are not considered here.

[44]T. Ohtsuki, Physica A **122**, 212 (1983).

[45]J. P. Gorcester, S. B. Rananavare, and J. H. Freed, J. Chem. Phys. **90**, 5764 (1989).

[46]D. S. Leniart, H. D. Connor, and J. H. Freed, J. Chem. Phys. **63**, 165 (1975).

[47]D. Chandler, *Introduction to Modern Statistical Mechanics* (Oxford University, New York, 1987).

[48]S. A. Zager and J. H. Freed, J. Chem. Phys. **77**, 3344 (1982).

[49]M. Tinkham, *Group Theory and Quantum Mechanics* (McGraw-Hill, New York, 1964).

[50]This assumes that the order parameter S for the spin probe is the same in the N and S_A phases. In fact, however, spin probes are known to undergo expulsion from ordered to disordered regions as smectic layers begin to form (Refs. 13 and 14).